Epigenetic regulation of *Wnt7b* expression by the *cis*-acting long noncoding RNA Lnc-Rewind in muscle stem cells

Andrea Cipriano[1†‡], Martina Macino[1,2†], Giulia Buonaiuto[1], Tiziana Santini[1,3], Beatrice Biferali[1,2], Giovanna Peruzzi[3], Alessio Colantoni[1], Chiara Mozzetta[2]*, Monica Ballarino[1]*

[1]Department of Biology and Biotechnology Charles Darwin, Sapienza University of Rome, Rome, Italy; [2]Institute of Molecular Biology and Pathology (IBPM), National Research Council (CNR) at Sapienza University of Rome, Rome, Italy; [3]Center for Life Nano Science@Sapienza, Istituto Italiano di Tecnologia, Rome, Italy

*For correspondence:
chiara.mozzetta@uniroma1.it (CM);
monica.ballarino@uniroma1.it (MB)

[†]These authors contributed equally to this work

Present address: [‡]Department of Obstetrics & Gynecology, Stanford University, Stanford, United States

Competing interests: The authors declare that no competing interests exist.

Abstract Skeletal muscle possesses an outstanding capacity to regenerate upon injury due to the adult muscle stem cell (MuSC) activity. This ability requires the proper balance between MuSC expansion and differentiation, which is critical for muscle homeostasis and contributes, if deregulated, to muscle diseases. Here, we functionally characterize a novel chromatin-associated long noncoding RNA (lncRNA), Lnc-Rewind, which is expressed in murine MuSCs and conserved in human. We find that, in mouse, Lnc-Rewind acts as an epigenetic regulator of MuSC proliferation and expansion by influencing the expression of skeletal muscle genes and several components of the WNT (Wingless-INT) signalling pathway. Among them, we identified the nearby Wnt7b gene as a direct Lnc-Rewind target. We show that Lnc-Rewind interacts with the G9a histone lysine methyltransferase and mediates the in cis repression of Wnt7b by H3K9me2 deposition. Overall, these findings provide novel insights into the epigenetic regulation of adult muscle stem cells fate by lncRNAs.

Introduction

The transcriptional output of all organisms was recently found to be more complex than originally imagined, as the majority of the genomic content is pervasively transcribed into a diverse range of regulatory short and long non-protein coding RNAs (ncRNAs) (*Abugessaisa et al., 2017*; *Carninci et al., 2005*; *Cipriano and Ballarino, 2018*). Among them, long noncoding RNAs (lncRNAs) are operationally defined as transcripts longer than 200 nucleotides, which display little or no protein coding potential. Since the initial discovery, numerous studies have demonstrated their contribution to many biological processes, including pluripotency, cell differentiation, and organism development (*Ballarino et al., 2016*; *Fatica and Bozzoni, 2014*). LncRNAs were demonstrated to regulate gene expression at transcriptional, post-transcriptional, or translational level. The function and the mechanisms of action are different and primarily depend on their (nuclear or cytoplasmic) subcellular localization (*Carlevaro et al., 2019*; *Rinn and Chang, 2012*; *Ulitsky and Bartel, 2013*). A large number of lncRNAs localize inside the nucleus, either enriched on the chromatin or restricted to specific nucleoplasmic foci (*Engreitz et al., 2016*; *Sun et al., 2018*). In this location, they have the capacity to control the expression of neighbouring (in cis) or distant (in trans) genes by regulating their chromatin environment and also acting as structural scaffolds of nuclear domains (*Kopp and Mendell, 2018*). Among the most important functions proposed for *cis*-acting lncRNAs, there is their ability to

regulate transcription by recruiting repressing or activating epigenetic complexes to specific genomic loci (*Huarte et al., 2010*; *Maamar et al., 2013*; *McHugh et al., 2015*; *Wang et al., 2011*).

In muscle, high-throughput transcriptome sequencing (RNA-seq) and differential expression analyses have facilitated the discovery of several lncRNAs that are modulated during the different stages of skeletal myogenesis and dysregulated in muscle disorders (*Ballarino et al., 2016*; *Lu et al., 2013*; *Zhao et al., 2019*). Although the roles of these transcripts have been partially identified, we are still far from a complete understanding of their mechanisms of action. For instance, the knowledge of the lncRNAs impact on adult muscle stem cell (MuSC) biology is partial and only a few examples have been characterized as functionally important. In the cytoplasm, the lncRNA *Lnc-mg* has been shown to regulate MuSC differentiation by acting as a sponge for *Mir125b* (*Zhu et al., 2017*). In the nucleus, the lncRNA *Dubr* was found to promote satellite cell differentiation by recruiting Dnmts to the developmental pluripotency-associated 2 (*Dppa2*) promoter, leading to CpG hypermethylation and silencing (*Wang et al., 2015*). In mouse, we have previously identified several lncRNAs specifically expressed during muscle in vitro differentiation and with either nuclear or cytoplasmic localization (*Ballarino et al., 2015*). Among them, we found Lnc-Rewind (**Re**pressor of **w**nt **ind**uction), a chromatin-associated lncRNA conserved in human and expressed in proliferating C_2C_{12} myoblasts.

Here, we provide evidence on the role of Lnc-Rewind in the epigenetic regulation of the WNT (Wingless-INT) signalling in muscle cells. The WNT transduction cascade has been demonstrated to act as a conserved regulator of stem cell function via canonical (β-CATENIN) and non-canonical (planar cell polarity and calcium) signalling, and dysregulation of its activity has been reported in various developmental disorders and diseases (*Nusse and Clevers, 2017*). In the muscle stem cell niche, WNT signalling is key in coordinating MuSC transitions from quiescence, proliferation, commitment, and differentiation (*Brack et al., 2008*; *Eliazer et al., 2019*; *Lacour et al., 2017*; *Le Grand et al., 2009*; *Parisi et al., 2015*; *Rudolf et al., 2016*). Because of this central role, the WNT pathway is supervised by several mechanisms and different works have shown that lncRNAs can modulate it at both transcriptional and post-transcriptional levels (*Zarkou et al., 2018*). Here, we provide evidence that Lnc-Rewind associates with the H3K9 methyltransferase G9a to regulate the deposition of H3K9me2 in cis on the nearby *Wnt7b* gene. Our data show that Lnc-Rewind expression is necessary to maintain *Wnt7b* repressed and to allow MuSC expansion and proper differentiation.

Results

Lnc-Rewind is a conserved chromatin-associated lncRNA expressed in satellite cells

In an attempt to uncover novel regulators of MuSC activity, we decided to take advantage of the atlas of newly discovered lncRNAs, which we previously identified as expressed in proliferating muscle cells (*Ballarino et al., 2015*). Among them, we focused on Lnc-Rewind, which is a lncRNA enriched in proliferating myoblasts and overlapping *pre-Mirlet7c-2* (*mmu-let7c-2*) and *pre-Mirlet7b* (*mmu-let7b*) genomic loci (*Figure 1A*). An evolutionary conservation analysis performed by examining FANTOM5 datasets (*Noguchi et al., 2017*) revealed the existence of a conserved transcriptional start site (TSS) localized in the human (hs_Lnc-Rewind) syntenic locus (*Figure 1B*). This region exhibits an overall ~46% of (exonic and intronic) sequence identity (*Figure 1—figure supplement 1A*), which is relatively high for lncRNAs. Moreover, RNA-seq (*Legnini et al., 2017*; *Figure 1B*) and semi-quantitative (sq)RT-PCR analyses (*Figure 1—figure supplement 1B*) confirmed that, in proliferating human myoblasts, this region is actively transcribed. To note, the distribution of the read coverage in both mouse and human revealed the existence of spliced and unspliced Lnc-Rewind isoforms originating from the two loci (*Figure 1A,B*).

To pinpoint possible roles of the murine transcript in muscle cells, we first assessed Lnc-Rewind expression and subcellular localization in both C_2C_{12} and Fluorescence-activated cell sorting (FACS) isolated MuSC (*Figure 1—figure supplement 1C*) grown under proliferative (hereafter referred to as MuSC-derived myoblasts) and differentiating conditions. Proper myogenic differentiation was confirmed by the expression of late muscle-specific genes such as myogenin (*Myog*) and muscle creatin kinase (*Mck*) (*Figure 1—figure supplement 1D*). Quantitative qRT-PCR analysis revealed that Lnc-Rewind expression is high in proliferating (GM) C_2C_{12} and MuSC-derived myoblasts and significantly decreased in fully differentiated (DM) cells (*Figure 1C*). Subcellular
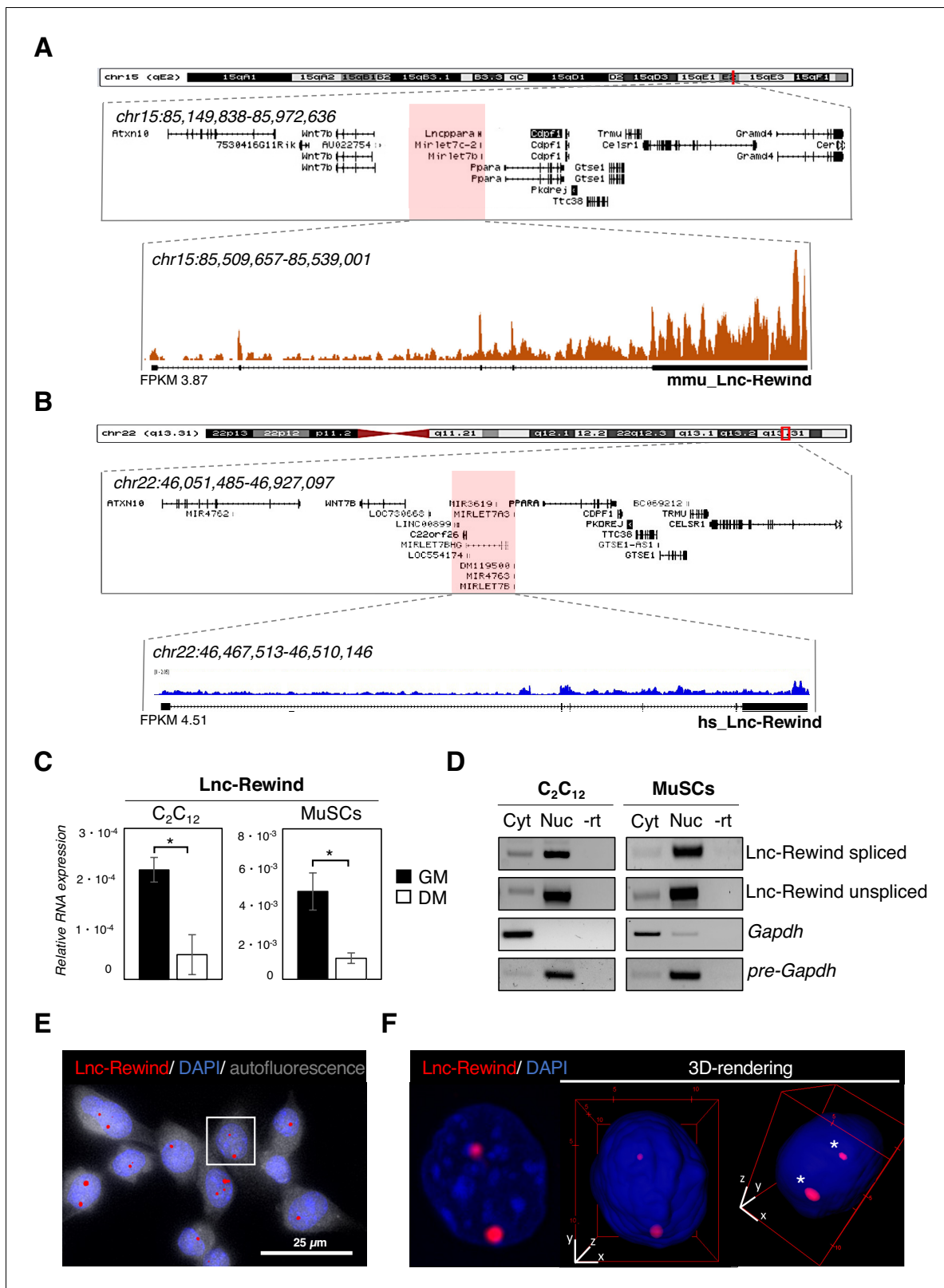
Figure 1. Lnc-Rewind is a conserved chromatin-associated lncRNA expressed in satellite cells. (**A**) UCSC visualization showing the chromosome position and the genomic coordinates of Lnc-Rewind (red shade) in the mm9 mouse genome. Mmu_Lnc-Rewind reads coverage and quantification (FPKM) from RNA-Seq experiments performed in proliferating C_2C_{12} cells (*Ballarino et al., 2015*; GSE94498) are shown. (**B**) UCSC visualization showing the chromosome position and the genomic coordinates of hs_Lnc-Rewind (red shade) in the hg19 human genome. Hs_Lnc-Rewind reads coverage and

Figure 1 continued on next page

quantification (FPKM) from RNA-Seq experiments performed in proliferating myoblasts (*Legnini et al., 2017*; GSE70389) are shown together with the genomic structure of the human locus (magnified box). (C) Relative Lnc-Rewind expression assessed by quantitative RT-PCR (qRT-PCR) in C$_2$C$_{12}$ myoblast (C$_2$C$_{12}$) and MuSC-derived myoblasts (referred as MuSCs) maintained in growing (GM) or differentiated (DM) conditions. Data represent the mean ± SEM from three biological replicates. *Gapdh* RNA was used as a normalization control. (D) Semiquantitative RT-PCR (sqRT-PCR) analysis of spliced and unspliced Lnc-Rewind isoforms in cytoplasmic (Cyt) and nuclear (Nuc) fractions from proliferating C$_2$C$_{12}$ and MuSC-derived myoblasts. The quality of fractionation was tested with mature (*Gapdh*) and precursor (*pre-Gapdh*) RNAs. –rt represents the negative control. (E) RNA-FISH analysis for Lnc-Rewind RNA (red) in proliferating MuSC-derived myoblasts. Autofluorescence (grey) is shown with false colour to visualize the cell body. (F) Digital magnification and 3D visualization of the square insert of (E). Asterisks indicate the Lnc-Rewind RNA signals inside the nuclear volume. DAPI, 4′,6-diamidino-2-phenylindole (blue). Data information: *p<0.05, unpaired Student's t-test.

The online version of this article includes the following source data and figure supplement(s) for figure 1:

Source data 1. Source data for Figure 1
Figure supplement 1. Lnc-Rewind is a conserved chromatin-associated lncRNA expressed in satellite cells.
Figure supplement 1—source data 1. Source data for Figure1-figure supplement 1.

fractionation of cytoplasmic (Cyt) and nuclear (Nuc) fractions showed that both spliced and unspliced isoforms localizes in the nuclear compartment (*Figure 1D*, *Figure 1—figure supplement 1E*). Accordingly, RNA fluorescence in situ hybridization (FISH) experiments performed in both MuSC-derived myoblasts (*Figure 1E,F*, *Figure 1—figure supplement 1F*) and C$_2$C$_{12}$ cells (*Figure 1—figure supplement 1G*) confirmed the nuclear localization of Lnc-Rewind and further revealed its specific enrichment to discrete chromatin foci. Overall, these results point towards a role for Lnc-Rewind in chromatin-based processes and suggest its possible involvement in the epigenetic regulation of MuSC homeostasis.

Lnc-Rewind regulates muscle system processes and MuSC expansion

To gain insights into the functional role of Lnc-Rewind and to identify the molecular pathways involved in the regulation of muscle stem cells, we performed a global transcriptional profiling on MuSC-derived myoblasts treated with either a mix of three different LNA GapmeRs against Lnc-Rewind (GAP-REW) or the scramble control (GAP-SCR) (*Figure 2—figure supplement 1A*, upper panel). Under these conditions, we obtained ~70% reduction of Lnc-Rewind expression (*Figure 2—figure supplement 1A*, lower panel), which led to the identification of a set of 1088 differentially expressed genes (DEGs) (p<0.05, GAP-SCR vs GAP-REW). Of these, 332 were upregulated and 756 downregulated in GAP-REW as compared to the GAP-SCR condition (*Figure 2A*, *Figure 2—source data 1*). A principal component analysis (PCA) performed on the DEG datasets revealed that the GAP-SCR and GAP-REW experimental groups displayed a clear different pattern of gene expression since they occupy different regions of the PCA plot (*Figure 2—figure supplement 1B*). The DEG list was then subjected to Gene Ontology (GO) term enrichment analysis (Biological process) to define functional clusters. It emerged that DEGs were mostly associated with muscle cell physiology (skeletal muscle contraction, p-value=4.23E-6) (*Figure 2B*, *Figure 2—figure supplement 1C*). Of note, the analysis of Lnc-Rewind generated miRNAs (*Mirlet7b* and *Mirlet7c-2*) revealed that, although the lncRNA depletion results on their concomitant downregulation (*Figure 2—figure supplement 1D*), none of the upregulated transcripts that are also putative *Mirlet7b* and *Mirlet7c-2* targets (~1% of the upregulated genes) (*Figure 2—figure supplement 1E*), belong to any of the GO enriched categories. This result emphasizes a specific and miRNA-independent role for Lnc-Rewind. Both 'muscle system process' (p-value=3.45E-7) and 'striated muscle contraction' (p-value=4.63E-7) were the most significantly enriched GO terms (*Figure 2—figure supplement 1C*). Of note, genes encoding for different proteins involved in muscle contraction, such as myosins (i.e. *Myh8*, *Myl1*, *Myh3*) and troponins (i.e. *Tnnt2*, *Tnnt1*) (*Figure 2C*), were downregulated. Accordingly, Lnc-Rewind-depleted cells express lower levels of MyHC protein (*Figure 2D*). Moreover, morphological evaluation highlighted a decreased number of MuSC-derived myoblasts after Lnc-Rewind depletion (*Figure 2—figure supplement 1F*), suggesting a primary defect in MuSC proliferation. This led us to hypothesize that the defects in myogenic capacity (*Figure 2C,D*, *Figure 2—figure supplement 1F*) might result by a decreased cell density that normally leads to a lower rate of myogenic differentiation. In line with this hypothesis, EdU incorporation experiments revealed a striking reduction of proliferating MuSC-derived myoblasts upon depletion of Lnc-Rewind (*Figure 2E*). Accordingly, the *Ccnd3* gene
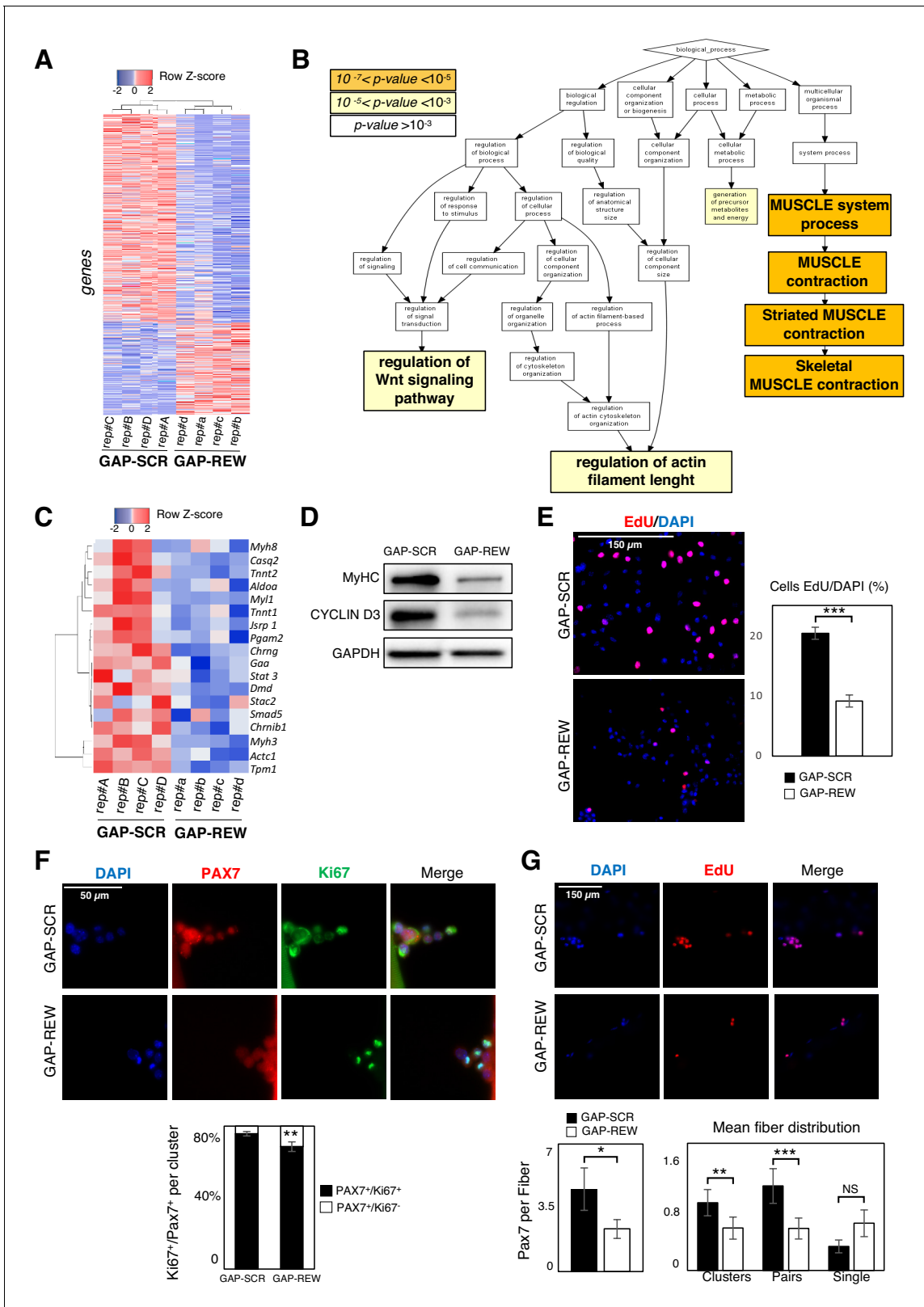
Figure 2. Lnc-Rewind regulates muscle system processes and MuSC expansion. (A) Heatmap representing hierarchical clustering performed on the final list of genes differentially expressed in MuSC-derived myoblasts upon Lnc-Rewind depletion (p-value threshold<0.05; see also *Figure 2—source data 1*). The analysis was performed using the Heatmapper webserver tool (Babicki et al., 2016). For each gene, expression levels are expressed as Z-score values. (B) Gene Ontology (GO) enrichment analysis performed by GORILLA (*Eden et al., 2009*) in Biological process for genes differentially expressed

Figure 2 continued on next page

upon Lnc-Rewind depletion in MuSC-derived myoblasts. (**C**) Heatmap representing hierarchical clustering performed on DEGs belonging to the Skeletal Muscle contraction GO category (GO:0003009). The analysis was performed using the Heatmapper webserver tool (Babicki et al., 2016). For each gene, expression levels are expressed as Z-score values. (**D**) Western blot analysis performed on protein extracts from MuSC-derived myoblasts treated with GAP-SCR or GAP-REW. GAPDH protein was used as endogenous control. (**E**) Representative images of MuSC-derived myoblasts treated with GAP-SCR and GAP-REW and incubated with EdU (red). Nuclei were visualized with DAPI (blue). Histogram shows the percentage of EdU-positive cells on the total of DAPI-positive cells. Data are graphed as mean ± SEM; n = 6 mice. (**F**) Representative images of single muscle fibres from WT mice treated with GAP-SCR or GAP-REW and stained for Pax7 (red) and Ki67 (green). Nuclei were visualized with DAPI (blue); histogram shows the percentage of Pax7$^+$/Ki67$^-$ cells on the total of Pax7$^+$/Ki67$^+$ cells per cluster. Data represent the mean ± SEM of 40 clusters per condition; n = 5 mice. (**G**) Representative images of single muscle fibres from WT mice treated with GAP-SCR or GAP-REW and incubated for 24 hr with EdU (red). Nuclei were visualized with DAPI (blue); left histogram shows the number of Pax7$^+$ cells per fibre (50 fibres per condition; n = 5 mice). Right histograms represent the mean of clusters (nuclei [n], n > 2), pairs (n = 2), and single cells Pax7$^+$ (n = 1) per fibre. Data represent the mean ± SEM of 80 fibres per condition; n = 5 mice. Data information: *p<0.05, **p<0.01, ***p<0.001, unpaired Student's t-test.

The online version of this article includes the following source data and figure supplement(s) for figure 2:

Source data 1. List of the Differentially Expressed Genes (DEGs) between GAP-SCR and GAP-REW transfected MuSCs.
Source data 2.Source data for Figure 2.
Figure supplement 1. Lnc-Rewind regulates muscle system processes and MuSC expansion.
**Figure supplement 1—source data 1. Source data for Figure 2-figure supplement 1.**

encoding for Cyclin D3, a cyclin specifically involved in promoting transition from G1 to S phase, was significantly downregulated in Lnc-Rewind-depleted cells at both transcript (*Figure 2—source data 1*) and protein levels (*Figure 2D*). In further support of this, MuSCs on single myofibres cultured for 96 hr gave rise to a decreased percentage of proliferating (Pax7$^+$/Ki67$^+$) progeny upon Lnc-Rewind downregulation (*Figure 2F*). Moreover, quantification of the number of Pax7$^+$-derived clusters (composed of more than two nuclei), pairs (composed of two nuclei), or single MuSCs within each myofibre revealed a reduction of activated pairs and clusters upon Lnc-Rewind depletion (*Figure 2G*), suggesting a role for the lncRNA in sustaining MuSC activation and expansion.

Lnc-Rewind and *Wnt7b* genes display opposite pattern of expression and a functional interplay

Together with the muscle-specific genes, the 'regulation of Wnt signalling pathway' GO term caught our attention as it was represented by a significant subset of trancripts (p-value=5.44E-4, *Figure 2—figure supplement 1C*). Among them, we found *Wnt7b*, which expression was found upregulated at both transcript and protein levels (*Figure 3—figure supplement 1A* and *Figure 2—source data 1*), suggesting a role for Lnc-Rewind as a repressor of *Wnt7b* expression. Intriguingly, *Wnt7b* transcriptional locus localizes only 100 kb upstream Lnc-Rewind gene (*Figure 3A*).

The genomic proximity between Lnc-Rewind/*Wnt7b* loci, together with their anti-correlated expression in muscle cells and the lncRNA chromatin enrichment (*Figure 1D,E*), led us to hypothesize that Lnc-Rewind might have a direct, in cis-regulatory role on *Wnt7b* transcription. A first clue in favour of such hypothesis came from FANTOM5 Cap Analysis Gene Expression (CAGE) profiles of mouse samples, available on ZENBU genome browser (*Noguchi et al., 2017*). Indeed, the inspection of the TSS usage among all the available murine samples (n = 1196, *Figure 3—source data 1*) revealed a distinctive anti-correlated expression between Lnc-Rewind and *Wnt7b* transcripts (*Figure 3B*, left panels). In contrast, the other Lnc-Rewind-neighbouring genes, such as *Cdpf1* and *Atxn10*, displayed no specific expression correlation (*Figure 3B*, right panels). Of note, *Wnt7b* was the only gene that was significantly upregulated upon the lncRNA depletion with a concomitant increase in WNT7b protein levels (*Figure 3C*, *Figure 3—figure supplement 1A,B*).

To uniquely link the defects in MuSC activation/proliferation induced by Lnc-Rewind depletion (*Figure 2E–G*) to the aberrant induction of *Wnt7b* expression, we performed a rescue experiment. To this end, in a context where the upregulation of *Wnt7b* was triggered by Lnc-Rewind depletion, we restored its expression to physiological levels by si-*Wnt7b*-mediated knockdown (*Figure 3—figure supplement 1C*). Of note, rescuing *Wnt7b* repression promoted an increase in the percentage of proliferating MuSC-derived myoblasts towards control levels (*Figure 3D*). Similarly, restoration of *Wnt7b* repression on single myofibres was sufficient to restore the capacity of the associated MuSCs to properly activate and proliferate ex vivo (*Figure 3E*), as assessed by the quantification of the
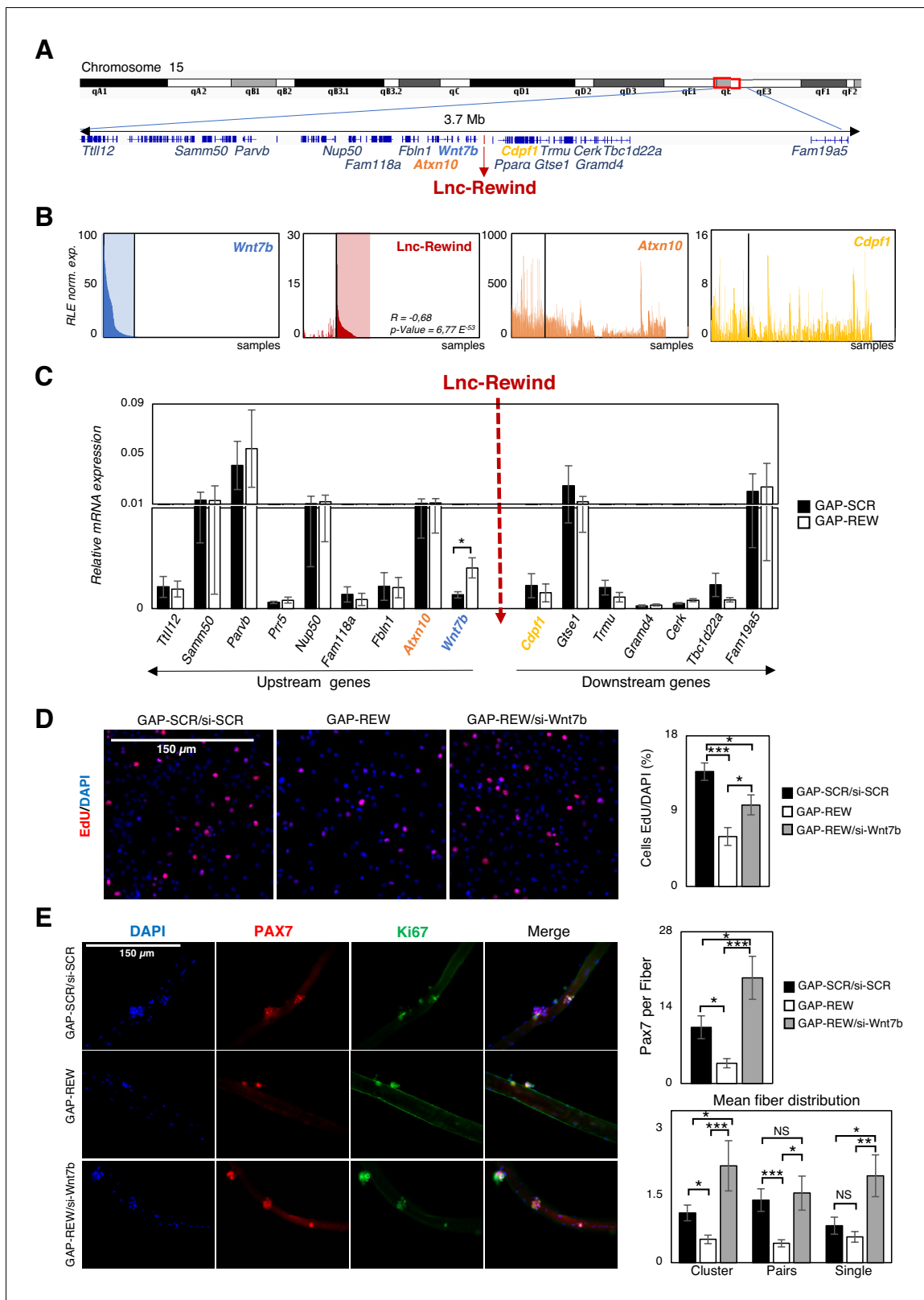
Figure 3. Lnc-Rewind and *Wnt7b* genes display opposite pattern of expression and a functional interplay. (**A**) Schematic UCSC visualization showing the Lnc-Rewind chromosome position and its neighbouring genes. (**B**) TSS usage analyses of *Wnt7b*, Lnc-Rewind, *Atxn10*, and *Cdpf1* performed by using FANTOM5 (Phases 1 and 2) CAGE datasets. Each bar represents the Relative Logarithmic Expression (RLE) of the tag per million (TPM) values of the TSS of each gene in one sample (1196 samples). The order of the samples is the same in each of the histograms and shown in ***Figure 3—source***

Figure 3 continued on next page

Figure 3 continued

data 1. R value represents the Spearman's rank correlation coefficient between Lnc-Rewind and *Wnt7b* expression, and the p-value was calculated using the Spearman's rank correlation test. (**C**) qRT-PCR quantification of Lnc-Rewind neighbouring genes in GAP-SCR *versus* GAP-REW treated MuSCs-derived myoblasts. Data were normalized to *Gapdh* mRNA and represent the average ± SEM from four biological replicates. (**D**) Representative images of MuSC-derived myoblasts treated with GAP-SCR/si-SCR, GAP-REW, and GAP-REW/si-Wnt7b and incubated with EdU (red). Nuclei were visualized with DAPI, 4′,6-diamidino-2-phenylindole (blue). Histogram shows the percentage of EdU-positive cells on the total of DAPI-positive cells. Data are graphed as mean ± SEM; n = 5 mice. (**E**) Representative images of single muscle fibres treated with GAP-SCR/si-SCR, GAP-REW, and GAP-REW/si-Wnt7b from WT mice after 96 hr in culture, stained for Pax7 (red) and Ki67 (green). Nuclei were visualized with DAPI, 4′,6-diamidino-2-phenylindole (blue). Histogram (upper panel) shows the number of Pax7$^+$ cells per fibre. Histograms (lower panel) represent the mean of the number of clusters (nuclei [n]: n > 2), pairs (n = 2), and single cells Pax7$^+$ (n = 1) per fibre. Data represent the mean ± SEM; n = 5 mice. Data information: (**C**): *$p<0.05$, paired Student's t-test. 3D and 3E: *$p<0.05$, **$p<0.01$, ***<0.001, one-way Anova with Tukey's multiple comparison test. The online version of this article includes the following source data and figure supplement(s) for figure 3:

Source data 1. 5′CAGE TSS expression profile of Wnt7b, Lnc-Rewind, Atxn10 and Cdpf1 genes.
Source data 2. Source data for Figure 3.
Figure supplement 1. Lnc-Rewind and *Wnt7b* genes display opposite pattern of expression and a functional interplay.
**Figure supplement 1—source data 1. Source data for Figure3-figure supplement 1.**

number of Pax7$^+$ MuSCs and the percentage of single MuSCs, and derived clusters and pairs, within each myofibre (*Figure 3E*). Together, these findings clearly candidate the Lnc-Rewind transcript as a regulator of *Wnt7b* repression in muscle stem cells and prompted us towards the study of the underlying mechanism by which this regulation occurs.

Lnc-Rewind directly interacts with the methyltransferase G9a and mediates specific in cis repression of *Wnt7b* in MuSCs

The above results suggest that Lnc-Rewind exerts a repressive role on *Wnt7b* gene expression. Several works accumulated so far indicate that most of the *cis*-acting chromatin-associated lncRNA function occurs by recruiting and guiding chromatin modifiers to target genes (*Batista and Chang, 2013*; *Guttman and Rinn, 2012*; *Khalil et al., 2009*; *Rinn and Chang, 2012*). In light of our data showing a negative correlation of *Wnt7b* expression by Lnc-Rewind, we focused our attention on the two most known repressive lysine methyltransferases, EZH2 and G9a, which catalyse the deposition of H3K27me3 and H3K9me1/2 on target genes, respectively (*Mozzetta et al., 2015*). Both EZH2 (*Caretti et al., 2004*) and G9a (*Ling et al., 2012*) are mostly expressed in proliferating MuSCs and become downregulated during muscle differentiation (*Figure 4—figure supplement 1A*), similarly to Lnc-Rewind (*Figure 1C*). Moreover, both EZH2 (*Rinn et al., 2007*; *Zhao et al., 2008*) and G9a (*Nagano et al., 2008*; *Pandey et al., 2008*) have been previously reported to be recruited to specific genomic loci through the interaction with different lncRNAs. Thus, we hypothesized that in proliferating myoblasts Lnc-Rewind might interact with EZH2 and/or G9a repressive complexes to tether them on *Wnt7b* genomic locus. Therefore, we performed RNA immunoprecipitation (RIP) analysis in proliferating C_2C_{12} cells using antibodies against G9a and EZH2. We observed that, although both G9a and EZH2 were successfully immunoprecipitated (*Figure 4—figure supplement 1B*, upper panel), Lnc-Rewind transcript was efficiently retrieved only in the G9a native RIP, while it was almost undetectable in EZH2 IP (*Figure 4—figure supplement 1B*, lower panel). To note, the levels of RNA obtained in the specific IP fraction were similar to the ones of the *Kcnq1ot1* lncRNA, which was previously demonstrated to be physically associated with both G9a and Ezh2 proteins (*Pandey et al., 2008*). The specificity of Lnc-Rewind and G9a interaction was strengthened by the use of two reciprocal strategies (*Figure 4*). On the one hand, the G9a-crosslinked immunoprecipitation (CLIP) assay (*Figure 4A*) revealed the presence of Lnc-Rewind in the G9a immunoprecipitated samples. As for RIP, also in this case, Lnc-Rewind RNA-specific enrichment was comparable to the *Kcnq1ot1*-positive control. As a further validation, endogenous Lnc-Rewind RNA pulldown (*Figure 4B*) revealed the presence of G9a in the lncRNA-precipitated fraction. This evidence confirmed the direct interaction between these two partners and led us to hypothesize that Lnc-Rewind might exert its repressive function on the *Wnt7b* locus through G9a. In support of this, depletion of G9a by siRNA-mediated knockdown in MuSC-derived myoblasts induced *Wnt7b* upregulation (*Figure 4C*). To test whether Lnc-Rewind and G9a binds the *Wnt7b* locus in vivo, we applied RNA-DNA-FISH (*Figure 4D*) and a chromatin immunoprecipitation (ChIP) assay (*Figure 4—figure*
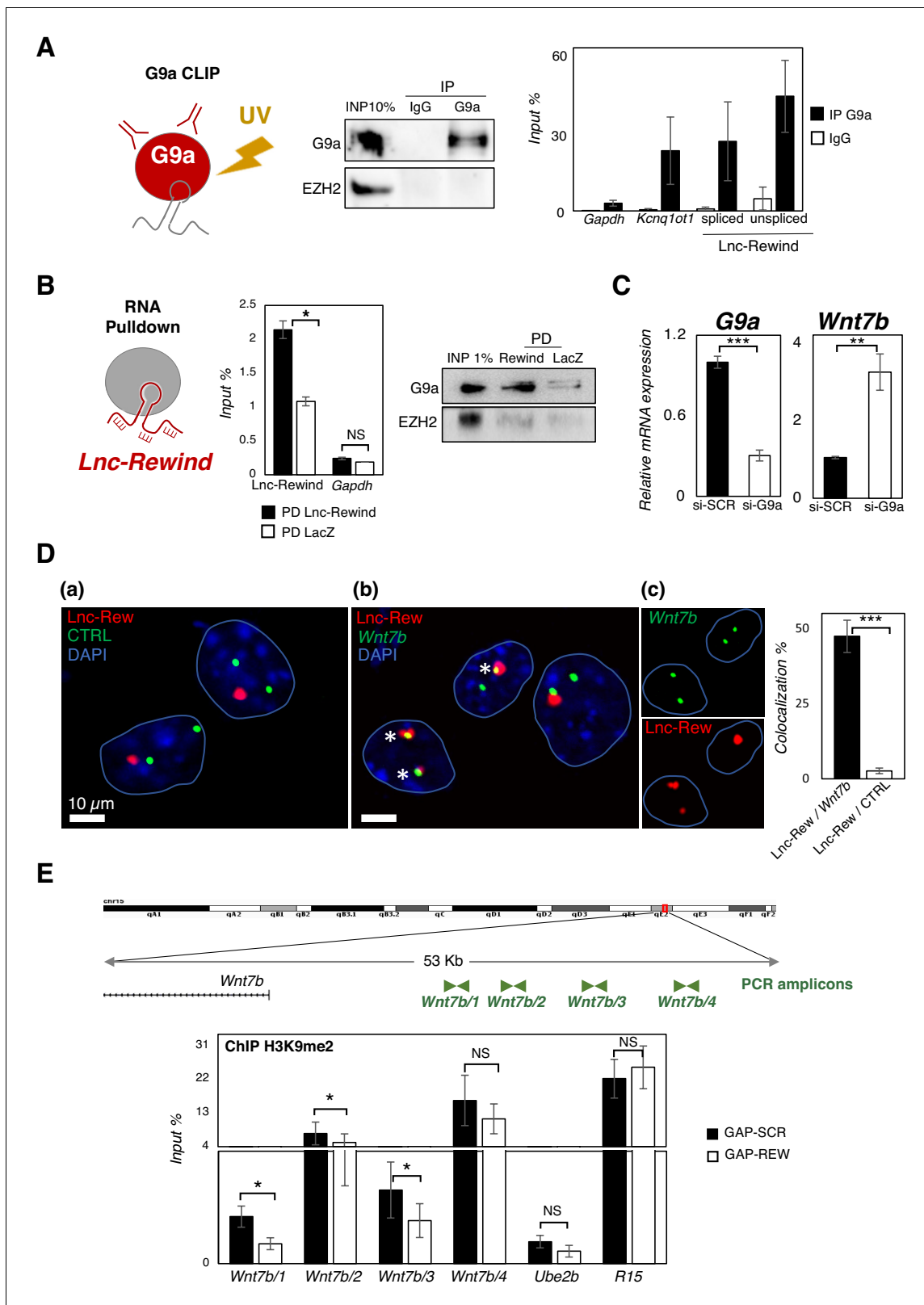
Figure 4. Lnc-Rewind directly interacts with the methyltransferase G9a and mediates specific in cis repression of *Wnt7b*. (**A**) G9a crosslinked RNA immunoprecipitation assay (CLIP) performed on nuclear extracts from C_2C_{12} proliferating myoblasts. Western blot analysis of G9a (left panel) and qRT-PCR quantification of Lnc-Rewind recovery (right panel) expressed as input percentage (Input %) are shown. EZH2 protein and *Gapdh* RNA serve as negative controls; *Kcnq1ot* RNA is used as positive control. Data represent mean ± SEM of three biological replicates. (**B**) Lnc-Rewind RNA pulldown

Figure 4 continued on next page

Figure 4 continued

assay performed on nuclear extracts from C_2C_{12} proliferating myoblasts. qRT-PCR quantification of Lnc-Rewind recovery (left panel) and Western blot analysis of G9a (right panel) are shown. *Gapdh* RNA and EZH2 protein serve as negative controls. Data represent mean ± SEM of three biological replicates. (C) qRT-PCR quantification of *G9a* and *Wnt7b* in MuSC-derived myoblasts treated with si-SCR or si-G9a. Data were normalized to *Gapdh* mRNA and represent the mean ± SEM of three biological replicates. (D) RNA/DNA-FISH experiments performed in proliferating MuSC-derived myoblasts showing the Lnc-Rewind RNA (red) and a DNA control (CTRL) region (green) (a) or the *Wnt7b* locus (green) (b). Inserts in (c) show single fluorescent channels for Lnc-Rewind and *Wnt7b* signals labelled by asterisks. Blue lines indicate the edges of the nuclei. DAPI, 4′,6-diamidino-2-phenylindole (blue). Histogram reports the mean percentage ± SD of Lnc-Rewind signals colocalizing with *Wnt7b* locus or with the control region from three biological replicates. The extended list of the DNA and RNA probes used is listed in Key resources table. (E) Zoom-in into the genomic region upstream the *Wnt7b* TSS (upper panel). ChIP amplicons used to test the H3K9me2 enrichments are shown in green. Histogram shows the levels of H3K9me2 as analysed by ChIP experiments performed in MuSC-derived myoblasts upon GAP-SCR or GAP-REW transfection (lower panel). The H3K9me2 enrichment is represented as input percentage (Input %). *Ube2b* and *R15* genomic regions were used as negative and positive controls, respectively. The graph shows the mean ± SEM of six independent experiments. Data information: (B) and (E): *p<0.05, paired Student's t-test. (C) and (D): **p<0.01, ***p<0.001, unpaired Student's t-test.

The online version of this article includes the following source data and figure supplement(s) for figure 4:

**Source data 1.** Source data for Figure 4.

Figure supplement 1. Lnc-Rewind directly interacts with the methyltransferase G9a and mediates specific in cis repression of *Wnt7b*.

Figure supplement 1—source data 1. Source data for Figure4-figure supplement 1.

supplement 1C), respectively. In agreement with our hypothesis, we found an overlap between Lnc-Rewind (RNA) and *Wnt7b* (DNA) localization (*Figure 4D*) and an intriguing enrichment of the methyl-transferase in the *Wnt7b* upstream regions (*Figure 4—figure supplement 1C*). Consistent with a role of Lnc-Rewind in the G9a-mediated epigenetic repression of *Wnt7b*, quantification of the H3K9me2 mark on the G9a-occupied genomic regions (*Figure 4E*, upper panel) showed that H3K9me2 deposition decreased upon Lnc-Rewind knockdown, compared to the GAP-SCR control (*Figure 4E*, lower panel). Moreover, a combined Lnc-Rewind (RNA)/*Wnt7b* (DNA) FISH/G9a (PRO-TEIN) immunostaining approach showed the colocalization of both G9a and Lnc-Rewind on *Wnt7b* genomic locus (*Figure 5A*). Taken together, these results support a mechanism of action through which in MuSC Lnc-Rewind represses *Wnt7b* gene transcription by mediating the specific G9a-dependent H3K9me2 deposition on its locus (*Figure 5B*).

Discussion

Wnt signalling represents one of the pathways that has a major role in myogenesis as it is essential for proper MuSC self-renewal and differentiation (*von Maltzahn et al., 2012*). A correct timing of Wnt signalling activation is crucial to obtain proper tissue repair, and its aberrant activity causes a wide range of pathologies (*Nusse and Clevers, 2017*). Thus, it is not surprising that Wnt pathway is under a strict positive and negative multi-layered regulation. Recent studies show that lncRNAs can modulate Wnt pathway by affecting gene expression through different mechanisms, from transcriptional to post-transcriptional level (*Ong et al., 2017*; *Shen et al., 2017*; *Zarkou et al., 2018*) For example, lncRNAs were found interacting with transcription factors (Di Cecilia et al. 2016) and chromatin modifiers (*Hu et al., 2015*) altering Wnt signalling pathway in different tissues and in cancer. In this study, we discovered that lncRNAs-mediated regulation plays a role in modulating Wnt pathway in muscle stem cells. Taking advantage of a newly discovered atlas of not annotated muscle-specific lncRNAs (*Ballarino et al., 2015*), we decided to focus our attention on Lnc-Rewind for the following reasons: (1) an orthologue transcript, hs_Lnc-Rewind, with high level of sequence identity is expressed by human myoblasts (*Figure 1B*, *Figure 1—figure supplement 1A,B*); (2) Lnc-Rewind is associated and retained to chromatin (*Figure 1D–F*); (3) it is in genomic proximity to *Wnt7b* locus (*Figure 3A*), and (4) its knockdown induces upregulation of *Wnt7b* in MuSC-derived myoblasts (*Figure 3C*, *Figure 3—figure supplement 1A,B*). Interestingly, the read coverage revealed the existence of multiple isoforms that are not fully spliced. The slowness in the splicing process could contribute to the maintenance of Lnc-Rewind at its own site of transcription improving its retention on the chromatin. In line with this, recent evidence indicates that the presence of introns, and their distinct processing, may represent a way to regulate the nuclear localization and function of many lncRNAs (*Guo et al., 2020*; *Zuckerman and Ulitsky, 2019*). These observations led us hypothesize a
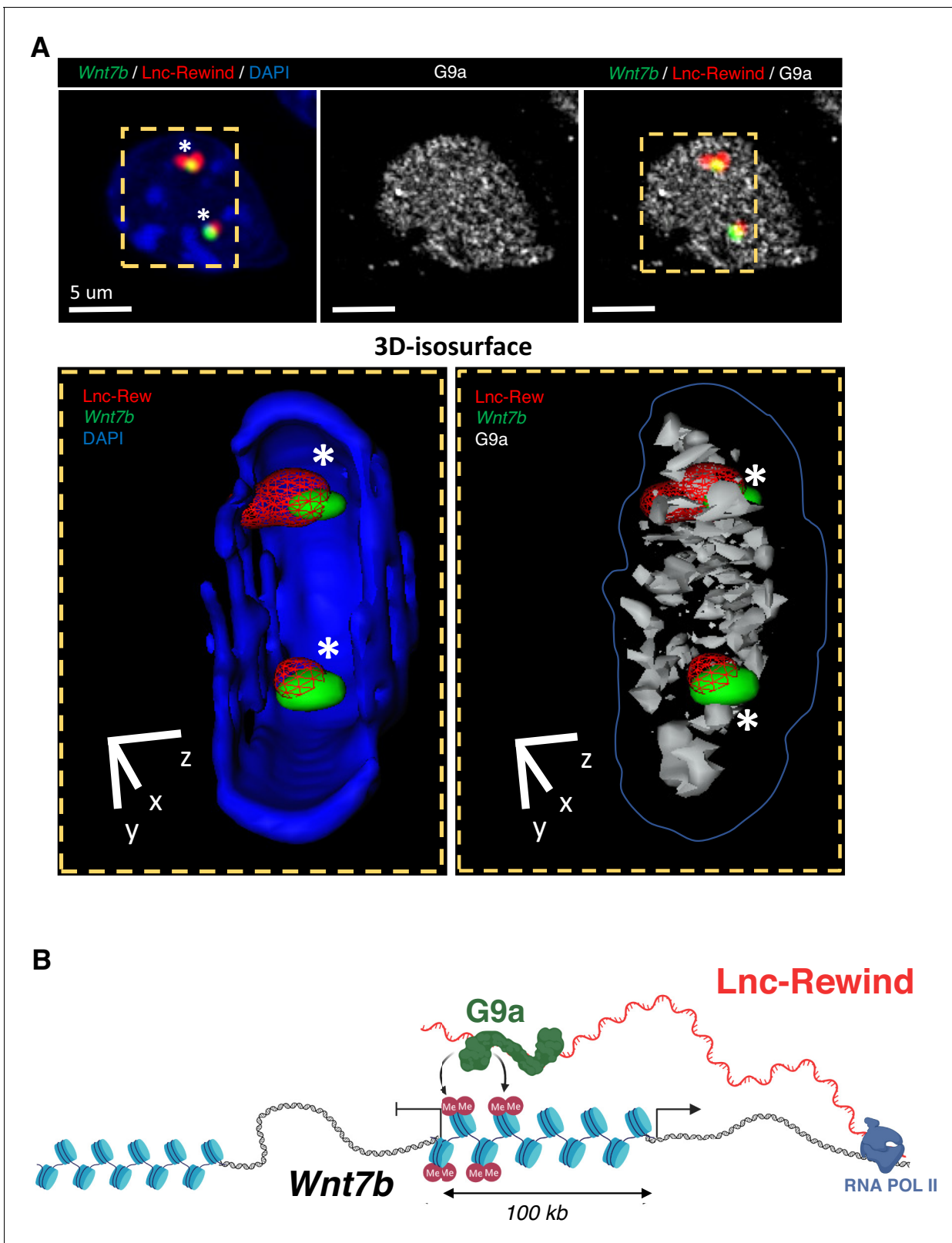
Figure 5. Lnc-Rewind and G9a colocalize on *Wnt7b* gene locus. (**A**) Top panel: RNA/DNA-FISH combined with immunofluorescence performed on MuSC-derived myoblasts; Lnc-Rewind RNA (red), *Wnt7b* DNA locus (green), and G9a protein (grey) are shown. Bottom panel: Isosurface rendering of nuclear sections is indicated by the yellow dashed lines. The overlapping regions between Lnc-Rewind (RNA) and *Wnt7b* (DNA) locus (left) and among Lnc-Rewind, *Wnt7b* locus, and G9a (right) are indicated by the white asterisks inside the nuclear volume. (**B**) Proposed model for the functional interplay

Figure 5 continued on next page

Lnc-Rewind-mediated in cis repression for *Wnt7b* gene. Of note, by analyzing the expression of surrounding genes within Lnc-Rewind genomic region, *Wnt7b* is the only gene to be significantly upregulated by Lnc-Rewind depletion (*Figure 3C*, *Figure 3—figure supplement 1B*). Moreover, we show that Lnc-Rewind and *Wnt7b* expressions are anti-correlated in different cell types (*Figure 3B*), suggesting that the repressive action of Lnc-Rewind on *Wnt7b* locus could have a more general role, not only in satellite cells.

It is well-accepted that the majority of the *cis*-acting chromatin-associated lncRNAs function by recruiting and targeting chromatin modifiers to specific genes (*Batista and Chang, 2013*; *Guttman and Rinn, 2012*; *Khalil et al., 2009*; *Rinn and Chang, 2012*). In light of the evidence that Lnc-Rewind promotes *Wnt7b* repression, we decided to investigate the involvement of the two major repressive histone modifiers, EZH2 and G9a, in mediating such Lnc-Rewind-dependent silencing. Notably, by performing both protein- and RNA-centric biochemical approaches (RIP/CLIP and RNA pulldown), we found that only G9a specifically interacts with Lnc-Rewind (*Figure 4A,B*, *Figure 4—figure supplement 1B*). This strongly suggests that the histone H3K9 lysine methyltransferase (KMT) might be specifically tethered on *Wnt7b* genomic locus by Lnc-Rewind to mediate its transcriptional repression. In support of this idea, through H3K9me2 ChIP experiments here we provide evidence that different regions upstream *Wnt7b* locus are enriched in the G9a-deposited histone mark in MuSC-derived myoblasts and that H3K9me2 levels on these regions significantly decrease upon Lnc-Rewind knockdown (*Figure 4E*). Moreover, both ChIP (*Figure 4—figure supplement 1C*) and imaging (*Figure 4D*) studies confirmed the presence of G9a in close proximity to *Wnt7b* locus. These data, together with the evidence that G9a downregulation is sufficient to induce *Wnt7b* de-repression (*Figure 4C*), confirm a direct role for G9a-mediated H3K9 methylation in maintaining the repression of *Wnt7b* in MuSCs.

A correct timing and magnitude of Wnt signalling activation is essential to maintain functional MuSCs. For instance, it has been shown that low β-catenin activity is fundamental during early phases of muscle regeneration to allow MuSC activation and subsequent differentiation (*Figeac and Zammit, 2015*; *Parisi et al., 2015*). Accordingly, satellite cells isolated from mice with constitutive active Wnt/β-catenin signalling display an early growth arrest and premature differentiation (*Rudolf et al., 2016*). All these data point out that the cell environment, together with the timing and the proper activation of Wnt signalling pathway, is fundamental for muscle homeostasis.

Although the function of WNT7b has been studied in different cell types and developmental processes (*Chen et al., 2014*; *Wang et al., 2005*), the involvement of this ligand in muscle biology is still rather unexplored. The fact that in MuSCs, *Wnt7b* gene is maintained at very low levels and that it is the latest Wnt ligand induced after muscle injury (*Polesskaya et al., 2003*) suggests the necessity to keep it repressed to allow MuSC expansion. In line with this, here we show that aberrant, cell-autonomous activation of *Wnt7b* expression upon Lnc-Rewind depletion causes defects in MuSC expansion and activation (*Figure 2E–G*) that are abolished if the expression of *Wnt7b* is rescued to physiological levels (*Figure 3D,E*), emphasizing that Lnc-Rewind-mediated repression of *Wnt7b* is key in ensuring MuSC activity. This is nicely supported by a previous study demonstrating that, in the cytoplasm, a *Wnt7b*/lncRNA circuitry controls the proliferation of C_2C_{12} myoblasts. Specifically, Lu and colleagues demonstrated that the YY1-associated muscle lincRNA (*Yam-1*) inhibits skeletal myogenesis through modulation of *Mir715* expression, which in turn targets *Wnt7b* mRNA (*Lu et al., 2013*). In sum, our results support a mechanism of action through which Lnc-Rewind mediates G9a recruitment on *Wnt7b* locus to silence it through the deposition of the repressive mark H3K9me2 during the proliferation phase of satellite cells (*Figure 5B*), thus providing unique insights on the contribution of nuclear-enriched lncRNAs in myogenesis.

Materials and methods

Key resources table

Reagent type (species) or resource	Designation	Source or reference	Identifiers	Addition
Strain, strain background (mouse)	C57Bl/10 (WT)	JAX	Stock# 000665 RRID:MGI:5656893	
Cell line (mouse)	C$_2$C$_{12}$	ATCC	C3H RRID:CVCL_UR38	
Cell line (human)	Male myoblast (WT)	Telethon Biobank	N/A	
Antibody	Anti-CD31-PE (cell line monoclonal)	MiltenyBiotec	Cat# 130111540 RRID:AB_2657296	(1:25)
Antibody	Anti-CD45-PE (cell line monoclonal)	MiltenyBiotec	Cat# 130110797 RRID:AB_2658218	(1:25)
Antibody	Anti-Ter119-PE (cell line monoclonal)	MiltenyBiotec	Cat# 130112909 RRID:AB_2654115	(1:25)
Antibody	Anti-Sca1-FITC (cell line monoclonal)	MiltenyBiotec	Cat# 130116490 RRID:AB_2751322	(1:50)
Antibody	Anti-α7Integrin-APCVio770 (cell line monoclonal)	MiltenyBiotec	Cat# 130095212 Custom	(1:20)
Antibody	Anti-G9a (rabbit monoclonal)	Abcam	Cat# ab185050 RRID:AB_2792982	(CLIP, RIF ChIP: 5 u WB: 1:10 IF: 1:100)
Antibody	Anti-EZH2 (mouse monoclonal)	Cell Signaling	Cat# 3147 RRID:AB_10694383	(RIP: 5 ug WB: 1:10
Antibody	Anti-GAPDH (rabbit polyclonal)	Sigma–Aldrich	Cat# G9545 RRID:AB_796208	(1:10000)
Antibody	Anti-MyHC (mouse monoclonal)	DSHB	Cat# Mf20-s RRID:AB_2147781	(1:20)
Antibody	Anti-CyclinD3 (rabbit polyclonal)	Santa Cruz Biotechnology	Cat# sc-182 RRID:AB_2259653	(1:200)
Antibody	Anti-Wnt7b (rabbit polyclonal)	Abcam	Cat#ab94915 RRID:AB_10675749	(1:200)
Antibody	Anti-H$_3$K$_9$me$_2$ (mouse monoclonal)	Abcam	Cat# ab1220 RRID:AB_449854	(ChIP: 5 u
Antibody	Anti-Pax7 (mouse monoclonal)	DSHB	Cat# Pax7-s RRID:AB_2299243	(1:10)
Antibody	IgG Anti-Rabbit	Invitrogen	Cat# 14-4616-82 RRID:AB_2865072	(CLIP, RIF ChIP: 5 u
Antibody	Donkey anti-rabbit IgG Alexa Fluor Plus 647	Invitrogen	Cat# A32795 RRID:AB_2762835	(1:300)
Antibody	Anti-Ki67 (rabbit polyclonal)	Abcam	Cat# ab15580 RRID:AB_443209	(1:100)
Sequence-based reagent	siRNA: nontargeting control	Sigma–Aldrich	Cat# SIC007	
Sequence-based reagent	LNA Gapmer: nontargeting control	Qiagen	Cat# 300610	
Sequence-based reagent	Mir-Let7-b	Qiagen	Cat# MS00003122	
Sequence-based reagent	Mir-Let7-c	Qiagen	Cat# 18300	
Sequence-based reagent	siG9a	Sigma–Aldrich	SASI_Mm01_00136174 SASI_Mm_00136174_AS SASI_Mm01_00136175 SASI_Mm01_00136175_AS	

Continued on next page

Continued

Reagent type (species) or resource	Designation	Source or reference	Identifiers	Addition
Sequence-based reagent	siWnt7b	Sigma–Aldrich	SASI_MM02_00316332 SASI_MM02_ 00316332_AS SASI_MM01_00033690 SASI_MM01_ 00033690_AS	
Sequence-based reagent	HS-DLC1 mRNA probe set	Advanced Cell Diagnostics, Inc	Ref. 716041	
Sequence-based reagent	Wnt7b BAC probe	Invitrogen clones	RP23-272K17	
Sequence-based reagent	NCTC BAC probe	Invitrogen clones	RP23-352B6	
Sequence-based reagent	Mm-Lnc-Rewind probe set	Advanced Cell Diagnostics, Inc	Ref. 722581	
Chemical compound, drug	TriReagent	Sigma	Cat#T9424	
Chemical compound, drug	DAPI	Sigma	Cat# 28718-90-3	(1:10000)
Chemical compound, drug	DSG (di-succinimidyl glutarate)	Santa Cruz Biotechnology	CAS 79642-50-5	
Commercial assay or kit	SYBR Green Master mix	ThermoFisher Scientific	Cat# A25742	
Commercial assay or kit	Paris Kit	Thermo fisher scientific	Cat# AM1921	
Commercial assay or kit	Direct-Zol RNA MiniPrep Kit	Zymo Research	Cat# R2050	
Commercial assay or kit	MAGnify ChIP	ThermoFisher Scientific	Cat# 492024	
Commercial assay or kit	MyTaq DNA polymerase	Bioline	Cat# bio-21105	
Commercial assay or kit	SuperScript RT Vilo Master Mix	ThermoFisher Scientific	Cat# 11754050	
Commercial assay or kit	BaseScope Reagent Kit v2-RED	Advanced Cell Diagnostics, Inc	Ref. 323900	
Commercial assay or kit	MiScript II RT kit	Qiagen	Cat# 218160	
Commercial assay or kit	Lipofectamine 2000	Invitrogen	Cat# 11668019	
Commercial assay or kit	Click-iT EdU Alexa Flour 594 HCS Assay	Invitrogen	Cat# C10354	
Commercial assay or kit	Pierce ChIP-grade Protein A/G Magnetic Beads	ThermoFisher scientific	Cat# 26162	
Peptide, recombinant protein	Dispase II	Roche	4942078001	
Peptide, recombinant protein	Proteinase K	Roche	EO0491	
Peptide, recombinant protein	Collagenase A	Roche	10103578001	
Peptide, recombinant protein	DNase I	Roche	10104159001	
Peptide, recombinant protein	DNase I	ThermoFisher scientific	#EN0521	
Peptide, recombinant protein	Collagenase I	Sigma	C0130	
Software, algorithm	FACSDiva	BD Biosciences	Version 6.1.3.	
Software, algorithm	FlowJo	Tree Star	Version 9.3.2 RRID:SCR_008520	

Continued on next page

Continued

Reagent type (species) or resource	Designation	Source or reference	Identifiers	Additior
Software, algorithm	Fiji image processing package	Open-source software (OSS) projects	https://imagej.net/Fiji RRID:SCR_002285	
Software, algorithm	MetaMorph	Molecular Devices	https://www.moleculardevices.com/ RRID:SCR_002368	
Software, algorithm	FV10-ASW Viewer software	Olympus	https://www.olympus-lifescience.com/ RRID:SCR_014215	
Software, algorithm	ZEN 3.0 Blue edition	ZEISS		

Cell preparation and FACS sorting

Cell isolation and labelling were essentially performed as described in *Mozzetta, 2016*. Isolation of cells from 2 months old C57/Bl10 (RRID:MGI:5656893) WT mice was performed as follows: briefly, whole lower hindlimb muscles were carefully isolated, minced, and digested in phosphate-buffered saline (PBS) (Sigma) supplemented with 2.4 U/ml Dispase II (Roche), 100 µg/ml Collagenase A (Roche), 50 mM $CaCl_2$, 1 M $MgCl_2$, 10 mg/ml DNase I (Roche) for 1 hr at 37°C under agitation. Muscle slurries were passed 10 times through a 20G syringe (BD Bioscience). Cell suspension was obtained after three successive cycles of straining and washing in Washing Buffer consisting of HBSS containing 0.2% bovine serum albumin (BSA) (Sigma–Aldrich), 1% penicillin-streptomycin. Cells were incubated with primary antibodies CD31-PE (MiltenyBiotec, 130111540; RRID:AB_2657296), CD45-PE (MiltenyBiotec, 139110797; RRID:AB_2658218), Ter119-PE (MiltenyBiotec, 130112909; RRID:AB_2654115) 1:25; Sca1-FITC (MiltenyBiotec, 130116490; RRID:AB_2751322) 1:50; α7Integrin-APC-Vio770 (MiltenyBiotec, 130095212; Custom) 1:20 for 45 min on ice diluted in HBSS containing 0.2% BSA, 1% penicillin-streptomycin, and 1% DNAse I. The suspension was finally washed and resuspended in PBS containing 2% fetal bovine serum (FBS) and 0.5 µM ethylenediaminetetraacetic acid (EDTA). Cells were sorted using a FACSAriaIII (Becton Dickinson, BD Biosciences) equipped with 488 nm, 561 nm, and 633 nm laser and FACSDiva software (BD Biosciences, version 6.1.3). Data were analyzed using a FlowJo software (Tree Star, version 9.3.2). Briefly, cells were first gated based on morphology using forward versus side scatter area parameter (FSC-A versus SSC-A) strategy followed by doublets exclusion with morphology parameter area versus width (A versus W). Muscle satellite cells (MuSCs) were isolated as $Ter119_{neg}/CD45_{neg}/CD31_{neg}/a7\text{-}integrin_{pos}/Sca1_{neg}$ cells. To reduce stress, cells were isolated in gentle conditions using a ceramic nozzle of size 100 µm, a low sheath pressure of 19.84 pound-force per square inch (psi) that maintain the sample pressure at 18.96 psi and a maximum acquisition rate of 3000 events/s. Cells were collected in five polypropylene tubes. Following isolation, an aliquot of the sorted cells was evaluated for purity at the same instrument resulting in an enrichment >98–99% (see *Figure 1—figure supplement 1C*, right panel).

Cell culture conditions and transfection

Freshly sorted cells were plated on ECM Gel (Sigma)-coated dishes in Cyto-grow (Resnova) complete medium as a growth medium (GM) and cultured at 37°C and 5% CO_2. After 5 days in GM, MuSC-derived myoblasts were exposed, generally for 2 days, to differentiation medium consisting of Dulbecco's modified Eagle's medium (DMEM) with 5% horse serum (HS). Cells were counted on DAPI-stained images using the Fiji (RRID:SCR_002285) tool 'Multi point'. Downregulation of RNA expression was performed at ~50% confluence by transfection in Lipofectamine 2000 (Invitrogen) according to manufacturer's instructions, with 75 nM of LNA GapmeRs (Euroclone) for the downregulation of Lnc-Rewind and with siRNA (Sigma) for *G9a* and *Wnt7b*, according to manufacturer's instructions. Negative Control A (Euroclone) (GAP-SCR) and Mission siRNA Universal Negative Control (Sigma) (si-SCR) were used as controls. See *Supplementary file 1* and Key resources table for details. MuSC-derived myoblasts were subjected to two consecutive (overnight) rounds of transfection in GM and harvested 24 hr after second transfection.

GapmeRs were designed against Lnc-Rewind sequence using the Exiqon web tool (http://www.exiqon.com/ls/Pages). Negative Control A (Euroclone) was used as negative (Scramble) control. Sequences are reported in *Supplementary file 1* and Key resources table.

For EdU (Invitrogen) detection cells were incubated for 6 hr and stained using Click-iT EdU Alexa Flour 594 HCS Assay (Invitrogen) according to the manufacturer's instructions.

Single myofibre isolation and immunofluorescence

Single myofibres were isolated from Extensor digitorum longus (EDL) muscles of C57/Bl10 mice and digested in 2 mg/ml collagenase I (Sigma) for 1 hr at 37°C, gently shacked every 10 min. Single fibres were obtained gently triturating the digested EDL muscles using a glass pipette in DMEM supplemented with 10% HS. The myofibres were manually collected under a dissecting microscope and cultured in DMEM + Pyr with 20% FBS, 2.5 ng/ml FGF (Gibco), and 1% chick embryo extract (CEE) (Life Science Production). RNAi experiments were performed 4 hr after plating with one round of transfection, as described above. The fibres were incubated for 24 hr with EdU (Invitrogen) and were analyzed 96 hr after plating.

For EdU detection cells were stained using Click-iT EdU Alexa Flour 594 HCS Assay (Invitrogen) according to the manufacturer's instructions.

For the immunofluorescence, the single myofibres were fixed with 4% paraformaldehyde in PBS for 20 min at room temperature (RT), permeabilized with 0.5% Triton X-100 in PBS, and blocked with 10% FBS in PBS for 1 hr at RT. Primary antibodies (Pax7 (DSHB, Pax7-s; RRID:AB_2299243) 1:10 and Ki67 (Abcam, ab15580; RRID:AB_443209) 1:100) were diluted in 10% FBS–PBS and incubated overnight at 4°C. After incubation for 1 hr with the appropriate secondary antibodies (Alexa Fluor 488 or 594, Thermo Fisher), nuclei were counterstained with DAPI (Sigma), and fibres were mounted on cover-glasses. Images were taken with Axio Observer microscope (ZEISS) and processed with ZEN 3.0 (Blue edition) software.

RNA/DNA-FISH

Lnc-Rewind in situ hybridization analyses were performed as previously described (*Rossi et al., 2019*). Briefly, proliferating MuSC-derived myoblasts and C_2C_{12} cells were cultured on pre-coated glass coverslips and then fixed in 4% paraformaldehyde/PBS (Electron Microscopy Sciences, Hatfield, PA). RNA hybridization and signal development were carried out using Basescope assay (Advanced Cell Diagnostics, Bio-Techne) and BA-Mm-Lnc-Rewind probe-set (ref. 722581) designed to detect three junction regions of Lnc-Rewind (exon/intron1, intron1/exon2, exon/intron2). A probe specific for exon junction exon1/exon2 of human Dlc1 mRNA (BA-HS-DLC1, ref. 716041) was used as negative control. Confocal images were acquired at Olympus IX73 spinning disk confocal microscope equipped with a Confocal Imager (CREST X-LIGHT) plus CoolSNAP Myo CCD camera (Photometrics) and at Olympus iX83 FluoView1200 laser scanning confocal microscope. Stacks of images were taken automatically with 0.2 or 0.3 microns between the Z-slices using a 60x NA1.35 oil objective and 405/473/559/635 nm or 405/470/555/640 nm lasers subset, respectively. Filter setting for DAPI, Alexa Fluor 488, Cy3, and Alexa Fluor 594 was used. The images were collected with MetaMorph or FV10-ASW confocal image acquisition software, and post-acquisition processing was performed by FIJI software to the entire image. 3D viewer plugin was used to perform 3D-rendering. DNA-FISH were sequentially carried out after RNA-FISH staining according to *Santini et al., 2021*. In particular, *Wnt7b* and negative control (corresponding to the *nctc* locus, previously used in Ballarino et al., 2018 and *Desideri et al., 2020*) genomic regions were visualized by nick-translated BAC clones (RP23-272K17 and RP23-352B6, respectively) labelled with Green 496 [5-fluorescein] dUTP (Enzo Life-Sciences). Percentage of colocalized signals in RNA/DNA-FISH experiments were measured as percentage ratio (%) of punctate Lnc-Rewind signals localized on the same focal plane of *Wnt7b* and negative control genomic regions, with respect to the total of Lnc-Rewind signals. In particular, we analysed a total of 135 nuclei for Lnc-Rewind/*Wnt7b* and 126 nuclei for Lnc-Rewind/negative control, from three independent biological replicates. G9a Immunofluorescence was performed sequentially to RNA-FISH staining by incubation in blocking solution (1% goat serum/1% BSA/PBS) for 30 min at RT. G9a primary antibody (Abcam, ab185050) was incubated in 1% donkey serum/PBS overnight at 4°C, while secondary antibody (donkey anti-rabbit Alexa Fluor Plus 647, Invitrogen A32795) were applied in the same incubation buffer for 45 min at RT.

RNA analyses

Total RNA from myoblasts/myotubes and MuSC-derived myoblasts was extracted with TriReagent (Sigma) using the Direct-Zol RNA MiniPrep Kit (Zymo Research) according to protocol specification. 0.5–1.0 µg of RNA were treated with RNase-free DNase I enzyme (Thermo scientific). Nuclear/cytoplasmic fractionation was performed using the Paris kit (Ambion, AM1921) according to the protocol specifications. RNA was reverse transcribed using the SuperScript VILO Master Mix (Thermo Scientific). Real-time quantitative PCRs were performed by using SYBR Green Master mix (Applied Biosystems), according to the manufacturer's instructions. Relative expression values were normalized to the housekeeping *Gapdh* transcript.

Western blot

Total proteins were prepared by resuspending cells in RIPA buffer (50 mM Tris–HCl pH 7.4, 150 mM NaCl, 0.1% sodium dodecyl sulphate (SDS), 0.5% sodium deoxycholate, 1% NP-40, 1 mM EDTA, protease and phosphatase inhibitors [Roche]). Protein concentration was determined using a BCA assay (ThermoFisher Scientific). The cell lysate was denatured at 95°C for 5 min. The cell lysates were resolved on 4–15% TGX gradient gels (Bio-Rad Laboratories) and transferred to nitrocellulose membrane (Amersham). Membranes were blocked with 5% non-fat dried milk in TBS with 0.2% Tween for 1 hr at RT and then incubated with primary antibody overnight at 4°C. Primary antibodies used were against MF20 (MyHC) (DSHB, Mf20-s; RRID:AB_2147781), G9a (Abcam, ab185050; RRID:AB_2792982), Ezh2 (Cell Signaling, #3147; RRID:AB_10694383), Wnt7b (Abcam, ab94915; RRID:AB_10675749), Cyclin D3 (Santa Cruz biotechnology, sc-182; RRID:AB_2259653), and GAPDH (Sigma, G9545; RRID:AB_796208). After washing in TBS with 0.2% Tween, membranes were incubated in HRP-conjugated specific secondary antibody (goat anti-rabbit-anti-mouse [IgG-HRP Santa Cruz Biotechnologies]) for 1 hr at RT. After washing in TBS with 0.2% Tween, blots were developed with Western lightning enhanced chemiluminescence (ThermoFisher Scientific), the signal detection was performed with the use of ChemiDoc (Bio-Rad).

RNA immunoprecipitation

C$_2$C$_{12}$ cells were washed with PBS, centrifuged at 2000 rpm for 5 min and resuspended in Buffer A (20 mM Tris–HCl pH 8.0, 10 mM NaCl, 3 mM MgCl$_2$, 0.1% NP40, 10% glycerol, 0.2 mM EDTA, 0.4 mM phenylmethylsulfonyl fluoride (PMSF), 1× Protease Inhibitor cocktail (PIC). After a 15 min incubation on ice, the cell suspension was centrifuged at 2000 rpm for 5 min at 4°C to pellet the nuclei. The supernatant was collected as cytoplasmic extract. The pellet was re-washed with Buffer A for three times. The pellet was resuspended in NT2/Wash buffer (50 mM Tris pH 7.4, 150 mM NaCl, 1 mM MgCl$_2$, 0.5% NP40, 20 mM EDTA, 1× PIC, 1× PMSF, 1 mM dithiothreitol [DTT]), break with 7 ml dounce (tight pestel/B pestel), and centrifuged at 14,000 rpm for 30 min at 4°C. Protein A/G Magnetic beads (Thermo Scientific) were incubate with IgG (Invitrogen, 14-4616-82; RRID:AB_2865072), G9a (Abcam, ab185050; RRID:AB_2792982), and Ezh2 (Cell Signaling, #3147; RRID:AB_10694383) antibody on rotating wheel ON at 4°C, while the nuclear extract (NE) was precleared with the beads. Ten percent of the NE was collected for INP. The NE was divided in each sample with the coated beads (beads + Ab) and incubates on rotating wheel ON at 4°C. The beads were washed with NT2 buffer, and ¼ was collected for protein and ¾ for RNA analyses. RIP qRT-PCR results were represented as percentage of IP/input signal (% input).

Crosslinking immunoprecipitation

CLIP experiments were performed on NE obtained with some modification of the Rinn et al.'s protocol (*Rinn et al., 2007*). Briefly, C$_2$C$_{12}$ cells were washed with PBS, crosslinked with UV rays and collected in Buffer A (20 mM Tris–HCl pH 8.0, 10 mM NaCl, 3 mM MgCl$_2$, 0.1% NP40, 10% glycerol, 0.2 mM EDTA, 0.4 mM PMSF, 1× PIC). Cells were centrifuged at 500 x g for 10 min and the supernatant was collected as cytoplasmic extract. The nuclei pellet was re-washed with Buffer A for three times. After the last wash, the nuclei pellet was resuspended in NP40 lysis buffer (50 mM HEPES–KOH, 150 Mm KCl, 2 Mm EDTA, 1 Mm NaF, 0.5% NP40 pH 7.4, 0.5 Mm DTT, 100× PIC), break with 7 ml dounce (tight pestel/B pestel) and centrifuged at maximum speed for 20 min at 4°C. The supernatant was collected and quantified with Bradford assay. Ten percent of the NE was collected for INP. Protein A/G Magnetic beads (Thermo Scientific) were washed with PBS Tween 0.02% (1× PBS,

0.02% Tween-20) and incubated in PBS Tween 0.02% with IgG (Invitrogen, 14-4616-82; RRID:AB_2865072) and G9a (Abcam, ab185050; RRID:AB_2792982) antibody on rotating wheel 1 hr at RT. The NE was divided in each sample with the coated beads (beads + Ab) and incubated on rotating wheel ON at 4°C. The beads were washed three times with the NP40 High Salt Buffer 0.5. (25 mM HEPES–KOH pH7.5, 250 mM KCl, 0.025% NP40) and two times with polynucleotide kinase PNK Buffer (50 mM Tris–HCL, 50 Mm NaCl, 10 mM $MgCl_2$ pH 7.5) and resuspended in 100 μl of NP40 lysis buffer. Seventy-five microlitres were collected for RNA analysis: an equal volume of 2× Proteinase K Buffer (100 mM Tris–HCl, pH 7.5, 150 mM NaCl, 12.5 mM EDTA, 2% [wt/vol] SDS) was added, followed by the addition of Proteinase K (Roche) to a final concentration of 1.2 mg/ml and incubated for 30 min at 55°C. The RNA was recovered and analyzed through qRT-PCR. Twenty-five microlitres were heated at 95°C for 5 min, and the supernatant collected and resuspended in Protein elution buffer (4× Laemmli sample buffer [Bio-Rad]) with DTT 50 mM and analyzed by Western blot.

RNA pulldown

RNA pulldown experiments were performed on NE obtained with some modification of the Rinn et al.'s protocol (*Rinn et al., 2007*). C_2C_{12} cells were washed with PBS and harvested in Buffer A (20 mM Tris–HCl pH 8.0, 10 mM NaCl, 3 mM $MgCl_2$, 0.1% NP40, 10% glycerol, 0.2 mM EDTA, 0.4 mM PMSF, 1× PIC). After a 15 min incubation on ice, they were centrifuged at 2000 rpm for 5 min at 4°C to pellet the nuclei. After three washes performed with Buffer A, the pellet was resuspended in NT2 buffer (50 mM Tris pH7.4, 150 mM NaCl, 1 mM $MgCl_2$, 0.5% NP40, 20 mM EDTA, 1× PIC, 1× PMSF, 1 mM DTT), broken with 1 ml dounce (tight pestel/B pestel) and centrifuged at 14,000 rpm for 30 min at 4°C. The supernatant was quantified with Bradford assay. Streptavidin magnetic beads (Promega) were incubated with biotinylated primers against Lnc-Rewind and LacZ on a rotating wheel for 30 min at RT, while the NE was precleared with the beads with the same conditions. One percent of the NE was collected for INP. The NE was divided in each sample with the coated beads (beads + primers) and incubated on rotating wheel for 2 hr at RT. The beads were washed with NT2 buffer and 1/5 was collected for the RNA. The remaining 4/5 were eluted in elution buffer (2% SDS, 10% glycerol, 62.5 mM Tris–HCl pH 7.5, 0.5 M DTT, 1× PIC) and incubated 15 min at 70° before incubation of 5 min at 90° in order to collect proteins. Pulldown (PD) qRT-PCR results were represented as percentage of PD/input signal (% input).

Chromatin immunoprecipitation

ChIP experiments on MuSC-derived myoblasts were performed on chromatin extracts according to the manufacturer's protocol (MAGnify ChIP; Life Technologies) by O.N. incubation with 3 μg of immobilized anti-H3K9me2 (Abcam ab1220; RRID:AB_449854) or rabbit IgG (14-4616-82; RRID:AB_2865072) antibodies. A standard curve was generated for each primer pair testing 5-point dilutions of input sample. Fold enrichment was quantified using qRT-PCR (SYBR Green; Qiagen) and calculated as a percentage of input chromatin (% Inp). Data from GAP-SCR vs GAP-REW conditions represent the mean of six independent experiments ± SEM. For G9a ChIP experiments on proliferating C_2C_{12}, crosslinking was performed by adding DSG (di-succinimidyl glutarate; Santa Cruz) at a final concentration of 2 mM for 45 min at RT. Then, formaldehyde (Sigma) was added to culture medium to a final concentration of 1% for 10 min at RT and stopped by glycine to a final concentration of 0.125 M. Chromatin was extracted as described in *Mozzetta et al., 2014* and immunoprecipitated with 5 μg of G9a (Abcam, ab185050; RRID:AB_2792982) or rabbit IgG (14-4616-82; RRID:AB_2865072) antibodies carried out overnight at 4°C. Sequences of the oligonucleotides used for ChIP analyses are reported in *Supplementary file 1*.

3′-End mRNA sequencing and bioinformatic analyses

Total RNA was quantified using the Qubit 2.0 Fluorimetric Assay (ThermoFisher Scientific). Libraries were prepared from 100 ng of total RNA using the QuantSeq 3′ mRNA-Seq Library Prep Kit FWD for Illumina (Lexogen GmbH); the quality was assessed by using screen tape high-sensitivity DNA D1000 (Agilent Technologies). Sequencing was performed on a NextSeq 500 using a high-output single-end, 75 cycles, v2 Kit (Illumina Inc). Illumina novaSeq base call (BCL) files were converted in fastq file through bcl2fastq (version v2.20.0.422). Sequence reads were trimmed using trimgalore (v0.4.1) to remove adapter sequences and low-quality end bases (regions with average quality below

Phred score 20). Alignment was performed with STAR 2.5.3a (*Dobin et al., 2013*) on mm10 reference. The expression levels of genes were determined with htseq-count 0.9.1 (*Anders et al., 2015*) by using mm10 Ensembl assembly (release 90). Genes having <1 count per million in at least four samples and those with a percentage of multi-mapping reads > 20% were filtered out. Paired t-test was performed to select differentially expressed genes in GAP-REW vs GAP-SCR conditions, setting 0.05 as p-value threshold. Gene Ontology term enrichment analyses were performed using GORILLA (*Eden et al., 2009*) by providing the list of genes expressed in at least one of the two conditions as background.

RNA-Seq reads from WT myoblasts cultured in GM (*Legnini et al., 2017*) were downloaded from GEO (GSE70389), preprocessed using Trimmomatic 0.32 software (*Bolger et al., 2014*), and aligned to human GRCh38 assembly using STAR 2.5.3a. The normalized read coverage tracks (.tdf files) were created and loaded on IGV genome browser (*Robinson et al., 2011*).

Statistical analyses

The statistical analyses were performed using Microsoft Excel (v16). The use of an unpaired or paired two-tailed Student's t-test is specified in each figure legend. For the data that did not show a normal distribution, the Spearman's rank correlation test was used. When more than two conditions were compared, one-way Anova with Tukey's multiple comparison test was applied using Prism (v9). Statistical significance was set at $p < 0.05$.

Acknowledgements

Additional information

Funding

Author contributions

Andrea Cipriano, Conceptualization, Data curation, Formal analysis, Supervision, Validation, Investigation, Visualization, Methodology, Writing - review and editing, Performed the cellular and molecular analyses in C2C12 cells, RNA-seq analysis, TSS usage, Gene Onthologies studies, ChIP experiments and the statistical analyses; Martina Macino, Conceptualization, Data curation, Formal analysis, Validation, Investigation, Visualization, Methodology, Writing - review and editing, performed the cellular and molecular experiments carried out on MuSCs and myofibers, RIP and CLIP on C2C12; Giulia Buonaiuto, Formal analysis, Validation, Visualization, contributed to the molecular analyses performed in C2C12 and MuSCs cells; Tiziana Santini, Methodology, performed RNA-FISH experiments; Beatrice Biferali, Methodology, contributed to the cellular experiments on MuSCs and myofibers; Giovanna Peruzzi, Methodology, perfomed FACS isolation of MuSCs; Alessio Colantoni,

Software, performed the bioinformatic analysis of the human myoblast RNA-seq; Chiara Mozzetta, Monica Ballarino, Conceptualization, Resources, Data curation, Supervision, Funding acquisition, Writing - original draft, Writing - review and editing

Author ORCIDs
Andrea Cipriano (iD) https://orcid.org/0000-0003-0775-3198
Martina Macino (iD) https://orcid.org/0000-0002-8730-9005
Giulia Buonaiuto (iD) https://orcid.org/0000-0002-4099-2433
Beatrice Biferali (iD) https://orcid.org/0000-0002-2399-885X
Chiara Mozzetta (iD) https://orcid.org/0000-0002-7147-7266
Monica Ballarino (iD) https://orcid.org/0000-0002-8595-7105

Ethics

Animal experimentation: For the experiments described in this study, C57/BL10 wild-type mice were used and differences which were observed in both male and female mice were included in experiments. Animals were treated in respect to housing, nutrition and care according to the guidelines of Good laboratory Practice (GLP). All experimental protocols (Protocol N° 7FF2C.4 -Authorization N° 746/2016-PR) were approved and conformed to the regulatory standards. All animals were kept in a temperature of 22°C ± 3°C with a humidity between 50% and 60%, in animal cages with at least 5 animals.

Decision letter and Author response

Decision letter https://doi.org/10.7554/eLife.54782.sa1
Author response https://doi.org/10.7554/eLife.54782.sa2

Additional files

Supplementary files

• Supplementary file 1. List and sequences of the oligonucleotides, LNA gapmers, and siRNAs used.

• Transparent reporting form

Data availability

Sequencing data have been deposited in GEO under accession code GSE141396. All data generated or analysed during this study are included in the manuscript and supporting files.

The following dataset was generated:

Author(s)	Year	Dataset title	Dataset URL	Database and Identifier
Cipriano A, Macino M, Buonaiuto G, Santini T, Biferali B, Colantoni A, Peruzzi G, Mozzetta C, Ballarino M	2021	3' mRNA-seq analysis from murine satellite cells upon lnc-Rewind knockdown	https://www.ncbi.nlm.nih.gov/geo/query/acc.cgi?acc=GSE141396	NCBI Gene Expression Omnibus, GSE141396

The following previously published datasets were used:

Author(s)	Year	Dataset title	Dataset URL	Database and Identifier
Ballarino M, Cazzella V, D'Andrea D, Grassi L, Bisceglie L, Cipriano A, Santini T, Pinnarò C, Morlando M, Tramontano A,	2014	Discovery of Novel LncRNA species differentially expressed during murine muscle differentiation	https://www.ebi.ac.uk/ena/browser/view/PRJEB6112	European Nucleotide Archive (ENA) accession number, PRJEB6112

Bozzoni I				
Legnini I, Briganti F, Sthandier O, Bozzoni I	2016	Gene expression profiling of human and murine in vitro muscle differentiation	https://www.ncbi.nlm.nih.gov/geo/query/acc.cgi?acc=GSE70389	NCBI Gene Expression Omnibus, GSE70389
Arner E, Daub CO, Vitting-Seerup K, Andersson R, Lilje B, Drablos F, Lennartsson A, Rönnerblad M, Hrydziuszko O, Vitezic M, Freeman CT, Alhendi A, Arner P, Axton R, Baillie JK, Beckhouse A	2015	Transcribed enhancers lead waves of coordinated transcription in transitioning mammalian cells	https://fantom.gsc.riken.jp/5/data/	FANTOM5 Consortium, fantom

References

Abugessaisa I, Noguchi S, Hasegawa A, Harshbarger J, Kondo A, Lizio M, Severin J, Carninci P, Kawaji H, Kasukawa T. 2017. FANTOM5 CAGE profiles of human and mouse reprocessed for GRCh38 and GRCm38 genome assemblies. *Scientific Data* **4**:170107. DOI: https://doi.org/10.1038/sdata.2017.107

Anders S, Pyl PT, Huber W. 2015. HTSeq–a Python framework to work with high-throughput sequencing data. *Bioinformatics* **31**:166–169. DOI: https://doi.org/10.1093/bioinformatics/btu638, PMID: 25260700

Ballarino M, Cazzella V, D'Andrea D, Grassi L, Bisceglie L, Cipriano A, Santini T, Pinnarò C, Morlando M, Tramontano A, Bozzoni I. 2015. Novel long noncoding RNAs (lncRNAs) in Myogenesis: a *miR-31* overlapping lncRNA transcript controls myoblast differentiation. *Molecular and Cellular Biology* **35**:728–736. DOI: https://doi.org/10.1128/MCB.01394-14, PMID: 25512605

Ballarino M, Morlando M, Fatica A, Bozzoni I. 2016. Non-coding RNAs in muscle differentiation and musculoskeletal disease. *Journal of Clinical Investigation* **126**:2021–2030. DOI: https://doi.org/10.1172/JCI84419

Ballarino M, Cipriano A, Tita R, Santini T, Desideri F, Morlando M, Colantoni A, Carrieri C, Nicoletti C, Musarò A, Carroll DO, Bozzoni I. 2018. Deficiency in the nuclear long noncoding RNA *charme* causes myogenic defects and heart remodeling in mice. *The EMBO Journal* **37**:e99697. DOI: https://doi.org/10.15252/embj.201899697, PMID: 30177572

Batista PJ, Chang HY. 2013. Long noncoding RNAs: cellular address codes in development and disease. *Cell* **152**:1298–1307. DOI: https://doi.org/10.1016/j.cell.2013.02.012, PMID: 23498938

Bolger AM, Lohse M, Usadel B. 2014. Trimmomatic: a flexible trimmer for illumina sequence data. *Bioinformatics* **30**:2114–2120. DOI: https://doi.org/10.1093/bioinformatics/btu170, PMID: 24695404

Brack AS, Conboy IM, Conboy MJ, Shen J, Rando TA. 2008. A temporal switch from notch to wnt signaling in muscle stem cells is necessary for normal adult myogenesis. *Cell Stem Cell* **2**:50–59. DOI: https://doi.org/10.1016/j.stem.2007.10.006, PMID: 18371421

Caretti G, Di Padova M, Micales B, Lyons GE, Sartorelli V. 2004. The polycomb Ezh2 methyltransferase regulates muscle gene expression and skeletal muscle differentiation. *Genes & Development* **18**:2627–2638. DOI: https://doi.org/10.1101/gad.1241904, PMID: 15520282

Carlevaro G, Lantos AB, Cánepa GE, de Los Milagros Cámara M, Somoza M, Buscaglia CA, Campetella O, Mucci J. 2019. Metabolic labeling of surface Neo-sialylglyconjugates catalyzed by Trypanosoma cruzi trans-Sialidase. *Methods in Molecular Biology* **1955**:135–146. DOI: https://doi.org/10.1007/978-1-4939-9148-8_10, PMID: 30868524

Carninci P, Kasukawa T, Katayama S, Gough J, Frith MC, Maeda N, Oyama R, Ravasi T, Lenhard B, Wells C, Kodzius R, Shimokawa K, Bajic VB, Brenner SE, Batalov S, Forrest AR, Zavolan M, Davis MJ, Wilming LG, Aidinis V, et al. 2005. The transcriptional landscape of the mammalian genome. *Science* **309**:1559–1563. DOI: https://doi.org/10.1126/science.1112014, PMID: 16141072

Chen J, Tu X, Esen E, Joeng KS, Lin C, Arbeit JM, Rüegg MA, Hall MN, Ma L, Long F. 2014. WNT7B promotes bone formation in part through mTORC1. *PLOS Genetics* **10**:e1004145. DOI: https://doi.org/10.1371/journal.pgen.1004145, PMID: 24497849

Cipriano A, Ballarino M. 2018. The Ever-Evolving concept of the gene: the use of RNA/Protein experimental techniques to understand genome functions. *Frontiers in Molecular Biosciences* **5**:20. DOI: https://doi.org/10.3389/fmolb.2018.00020, PMID: 29560353

Dobin A, Davis CA, Schlesinger F, Drenkow J, Zaleski C, Jha S, Batut P, Chaisson M, Gingeras TR. 2013. STAR: ultrafast universal RNA-seq aligner. *Bioinformatics* **29**:15–21. DOI: https://doi.org/10.1093/bioinformatics/bts635, PMID: 23104886

Eden E, Navon R, Steinfeld I, Lipson D, Yakhini Z. 2009. GOrilla: a tool for discovery and visualization of enriched GO terms in ranked gene lists. *BMC Bioinformatics* **10**:48. DOI: https://doi.org/10.1186/1471-2105-10-48, PMID: 19192299

Eliazer S, Muncie JM, Christensen J, Sun X, D'Urso RS, Weaver VM, Brack AS. 2019. Wnt4 from the niche controls the Mechano-Properties and quiescent state of muscle stem cells. *Cell Stem Cell* **25**:654–665. DOI: https://doi.org/10.1016/j.stem.2019.08.007, PMID: 31495781

Engreitz JM, Haines JE, Perez EM, Munson G, Chen J, Kane M, McDonel PE, Guttman M, Lander ES. 2016. Local regulation of gene expression by lncRNA promoters, transcription and splicing. *Nature* **539**:452–455. DOI: https://doi.org/10.1038/nature20149, PMID: 27783602

Fatica A, Bozzoni I. 2014. Long non-coding RNAs: new players in cell differentiation and development. *Nature Reviews Genetics* **15**:7–21. DOI: https://doi.org/10.1038/nrg3606, PMID: 24296535

Figeac N, Zammit PS. 2015. Coordinated action of Axin1 and Axin2 suppresses β-catenin to regulate muscle stem cell function. *Cellular Signalling* **27**:1652–1665. DOI: https://doi.org/10.1016/j.cellsig.2015.03.025, PMID: 25866367

Guo C-J, Ma X-K, Xing Y-H, Zheng C-C, Xu Y-F, Shan L, Zhang J, Wang S, Wang Y, Carmichael GG, Yang L, Chen L-L. 2020. Distinct processing of lncRNAs contributes to Non-conserved functions in stem cells. *Cell* **181**:621–636. DOI: https://doi.org/10.1016/j.cell.2020.03.006

Guttman M, Rinn JL. 2012. Modular regulatory principles of large non-coding RNAs. *Nature* **482**:339–346. DOI: https://doi.org/10.1038/nature10887, PMID: 22337053

Hu P, Chu J, Wu Y, Sun L, Lv X, Zhu Y, Li J, Guo Q, Gong C, Liu B, Su S. 2015. NBAT1 suppresses breast Cancer metastasis by regulating DKK1 via PRC2. *Oncotarget* **6**:32410–32425. DOI: https://doi.org/10.18632/oncotarget.5609, PMID: 26378045

Huarte M, Guttman M, Feldser D, Garber M, Koziol MJ, Kenzelmann-Broz D, Khalil AM, Zuk O, Amit I, Rabani M, Attardi LD, Regev A, Lander ES, Jacks T, Rinn JL. 2010. A large intergenic noncoding RNA induced by p53 mediates global gene repression in the p53 response. *Cell* **142**:409–419. DOI: https://doi.org/10.1016/j.cell.2010.06.040, PMID: 20673990

Khalil AM, Guttman M, Huarte M, Garber M, Raj A, Rivea Morales D, Thomas K, Presser A, Bernstein BE, van Oudenaarden A, Regev A, Lander ES, Rinn JL. 2009. Many human large intergenic noncoding RNAs associate with chromatin-modifying complexes and affect gene expression. *PNAS* **106**:11667–11672. DOI: https://doi.org/10.1073/pnas.0904715106, PMID: 19571010

Kopp F, Mendell JT. 2018. Functional classification and experimental dissection of long noncoding RNAs. *Cell* **172**:393–407. DOI: https://doi.org/10.1016/j.cell.2018.01.011, PMID: 29373828

Lacour F, Vezin E, Bentzinger CF, Sincennes MC, Giordani L, Ferry A, Mitchell R, Patel K, Rudnicki MA, Chaboissier MC, Chassot AA, Le Grand F. 2017. R-spondin1 controls muscle cell fusion through dual regulation of antagonistic wnt signaling pathways. *Cell Reports* **18**:2320–2330. DOI: https://doi.org/10.1016/j.celrep.2017.02.036, PMID: 28273449

Le Grand F, Jones AE, Seale V, Scimè A, Rudnicki MA. 2009. Wnt7a activates the planar cell polarity pathway to drive the symmetric expansion of satellite stem cells. *Cell Stem Cell* **4**:535–547. DOI: https://doi.org/10.1016/j.stem.2009.03.013, PMID: 19497282

Legnini I, Di Timoteo G, Rossi F, Morlando M, Briganti F, Sthandier O, Fatica A, Santini T, Andronache A, Wade M, Laneve P, Rajewsky N, Bozzoni I. 2017. Circ-ZNF609 is a circular RNA that can be translated and functions in myogenesis. *Molecular Cell* **66**:22–37. DOI: https://doi.org/10.1016/j.molcel.2017.02.017

Ling BM, Bharathy N, Chung TK, Kok WK, Li S, Tan YH, Rao VK, Gopinadhan S, Sartorelli V, Walsh MJ, Taneja R. 2012. Lysine methyltransferase G9a methylates the transcription factor MyoD and regulates skeletal muscle differentiation. *PNAS* **109**:841–846. DOI: https://doi.org/10.1073/pnas.1111628109, PMID: 22215600

Lu L, Sun K, Chen X, Zhao Y, Wang L, Zhou L, Sun H, Wang H. 2013. Genome-wide survey by ChIP-seq reveals YY1 regulation of lincRNAs in skeletal myogenesis. *The EMBO Journal* **32**:2575–2588. DOI: https://doi.org/10.1038/emboj.2013.182

Maamar H, Cabili MN, Rinn J, Raj A. 2013. linc-HOXA1 is a noncoding RNA that represses Hoxa1 transcription in Cis. *Genes & Development* **27**:1260–1271. DOI: https://doi.org/10.1101/gad.217018.113, PMID: 23723417

McHugh CA, Chen CK, Chow A, Surka CF, Tran C, McDonel P, Pandya-Jones A, Blanco M, Burghard C, Moradian A, Sweredoski MJ, Shishkin AA, Su J, Lander ES, Hess S, Plath K, Guttman M. 2015. The xist lncRNA interacts directly with SHARP to silence transcription through HDAC3. *Nature* **521**:232–236. DOI: https://doi.org/10.1038/nature14443, PMID: 25915022

Mozzetta C, Pontis J, Fritsch L, Robin P, Portoso M, Proux C, Margueron R, Ait-Si-Ali S. 2014. The histone H3 lysine 9 methyltransferases G9a and GLP regulate polycomb repressive complex 2-mediated gene silencing. *Molecular Cell* **53**:277–289. DOI: https://doi.org/10.1016/j.molcel.2013.12.005, PMID: 24389103

Mozzetta C, Boyarchuk E, Pontis J, Ait-Si-Ali S. 2015. Sound of silence: the properties and functions of repressive lys methyltransferases. *Nature Reviews Molecular Cell Biology* **16**:499–513. DOI: https://doi.org/10.1038/nrm4029, PMID: 26204160

Mozzetta C. 2016. Isolation and culture of muscle stem cells. *Jove* **1480**:50846. DOI: https://doi.org/10.3791/50846

Nagano T, Mitchell JA, Sanz LA, Pauler FM, Ferguson-Smith AC, Feil R, Fraser P. 2008. The air noncoding RNA epigenetically silences transcription by targeting G9a to chromatin. *Science* **322**:1717–1720. DOI: https://doi.org/10.1126/science.1163802, PMID: 18988810

Noguchi S, Arakawa T, Fukuda S, Furuno M, Hasegawa A, Hori F, Ishikawa-Kato S, Kaida K, Kaiho A, Kanamori-Katayama M, Kawashima T, Kojima M, Kubosaki A, Manabe RI, Murata M, Nagao-Sato S, Nakazato K, Ninomiya N, Nishiyori-Sueki H, Noma S, et al. 2017. FANTOM5 CAGE profiles of human and mouse samples. *Scientific Data* **4**:170112. DOI: https://doi.org/10.1038/sdata.2017.112, PMID: 28850106

Nusse R, Clevers H. 2017. Wnt/β-Catenin signaling, disease, and emerging therapeutic modalities. *Cell* **169**:985–999. DOI: https://doi.org/10.1016/j.cell.2017.05.016, PMID: 28575679

Ong MS, Cai W, Yuan Y, Leong HC, Tan TZ, Mohammad A, You ML, Arfuso F, Goh BC, Warrier S, Sethi G, Tolwinski NS, Lobie PE, Yap CT, Hooi SC, Huang RY, Kumar AP. 2017. 'Lnc'-ing Wnt in female reproductive cancers: therapeutic potential of long non-coding RNAs in Wnt signalling. *British Journal of Pharmacology* **174**:4684–4700. DOI: https://doi.org/10.1111/bph.13958, PMID: 28736855

Pandey RR, Mondal T, Mohammad F, Enroth S, Redrup L, Komorowski J, Nagano T, Mancini-Dinardo D, Kanduri C. 2008. Kcnq1ot1 antisense noncoding RNA mediates lineage-specific transcriptional silencing through chromatin-level regulation. *Molecular Cell* **32**:232–246. DOI: https://doi.org/10.1016/j.molcel.2008.08.022, PMID: 18951091

Parisi A, Lacour F, Giordani L, Colnot S, Maire P, Le Grand F. 2015. APC is required for muscle stem cell proliferation and skeletal muscle tissue repair. *Journal of Cell Biology* **210**:717–726. DOI: https://doi.org/10.1083/jcb.201501053

Polesskaya A, Seale P, Rudnicki MA. 2003. Wnt signaling induces the myogenic specification of resident CD45+ adult stem cells during muscle regeneration. *Cell* **113**:841–852. DOI: https://doi.org/10.1016/S0092-8674(03)00437-9, PMID: 12837243

Rinn JL, Kertesz M, Wang JK, Squazzo SL, Xu X, Brugmann SA, Goodnough LH, Helms JA, Farnham PJ, Segal E, Chang HY. 2007. Functional demarcation of active and silent chromatin domains in human HOX loci by noncoding RNAs. *Cell* **129**:1311–1323. DOI: https://doi.org/10.1016/j.cell.2007.05.022, PMID: 17604720

Rinn JL, Chang HY. 2012. Genome regulation by long noncoding RNAs. *Annual Review of Biochemistry* **81**:145–166. DOI: https://doi.org/10.1146/annurev-biochem-051410-092902, PMID: 22663078

Robinson JT, Thorvaldsdóttir H, Winckler W, Guttman M, Lander ES, Getz G, Mesirov JP. 2011. Integrative genomics viewer. *Nature Biotechnology* **29**:24–26. DOI: https://doi.org/10.1038/nbt.1754, PMID: 21221095

Rossi F, Legnini I, Megiorni F, Colantoni A, Santini T, Morlando M, Di Timoteo G, Dattilo D, Dominici C, Bozzoni I. 2019. Circ-ZNF609 regulates G1-S progression in Rhabdomyosarcoma. *Oncogene* **38**:3843–3854. DOI: https://doi.org/10.1038/s41388-019-0699-4, PMID: 30670781

Rudolf A, Schirwis E, Giordani L, Parisi A, Lepper C, Taketo MM, Le Grand F. 2016. β-Catenin activation in muscle progenitor cells regulates tissue repair. *Cell Reports* **15**:1277–1290. DOI: https://doi.org/10.1016/j.celrep.2016.04.022, PMID: 27134174

Santini T, Martone J, Ballarino M. 2021. Visualization of nuclear and cytoplasmic long noncoding RNAs at Single-Cell level by RNA-FISH. *Methods in Molecular Biology* **2157**:251–280. DOI: https://doi.org/10.1007/978-1-0716-0664-3_15, PMID: 32820409

Shen P, Pichler M, Chen M, Calin G, Ling H. 2017. To wnt or lose: the missing Non-Coding linc in colorectal Cancer. *International Journal of Molecular Sciences* **18**:2003. DOI: https://doi.org/10.3390/ijms18092003

Sun Q, Hao Q, Prasanth KV. 2018. Nuclear long noncoding RNAs: key regulators of gene expression. *Trends in Genetics* **34**:142–157. DOI: https://doi.org/10.1016/j.tig.2017.11.005, PMID: 29249332

Ulitsky I, Bartel DP. 2013. lincRNAs: genomics, evolution, and mechanisms. *Cell* **154**:26–46. DOI: https://doi.org/10.1016/j.cell.2013.06.020, PMID: 23827673

von Maltzahn J, Chang NC, Bentzinger CF, Rudnicki MA. 2012. Wnt signaling in myogenesis. *Trends in Cell Biology* **22**:602–609. DOI: https://doi.org/10.1016/j.tcb.2012.07.008, PMID: 22944199

Wang Z, Shu W, Lu MM, Morrisey EE. 2005. Wnt7b activates canonical signaling in epithelial and vascular smooth muscle cells through interactions with Fzd1, Fzd10, and LRP5. *Molecular and Cellular Biology* **25**:5022–5030. DOI: https://doi.org/10.1128/MCB.25.12.5022-5030.2005

Wang KC, Yang YW, Liu B, Sanyal A, Corces-Zimmerman R, Chen Y, Lajoie BR, Protacio A, Flynn RA, Gupta RA, Wysocka J, Lei M, Dekker J, Helms JA, Chang HY. 2011. A long noncoding RNA maintains active chromatin to coordinate homeotic gene expression. *Nature* **472**:120–124. DOI: https://doi.org/10.1038/nature09819, PMID: 21423168

Wang L, Zhao Y, Bao X, Zhu X, Kwok YK, Sun K, Chen X, Huang Y, Jauch R, Esteban MA, Sun H, Wang H. 2015. LncRNA dum interacts with dnmts to regulate Dppa2 expression during myogenic differentiation and muscle regeneration. *Cell Research* **25**:335–350. DOI: https://doi.org/10.1038/cr.2015.21, PMID: 25686699

Zarkou V, Galaras A, Giakountis A, Hatzis P. 2018. Crosstalk mechanisms between the WNT signaling pathway and long non-coding RNAs. *Non-Coding RNA Research* **3**:42–53. DOI: https://doi.org/10.1016/j.ncrna.2018.04.001, PMID: 30159439

Zhao J, Sun BK, Erwin JA, Song JJ, Lee JT. 2008. Polycomb proteins targeted by a short repeat RNA to the mouse X chromosome. *Science* **322**:750–756. DOI: https://doi.org/10.1126/science.1163045, PMID: 18974356

Zhao Y, Chen M, Lian Z, Li Y, Li Y, Wang J, Deng S, Kun Y, Lian Z. 2019. Non-Coding RNA regulates the myogenesis of skeletal muscle satellite cells, injury repair and diseases. *Cells* **8**:988. DOI: https://doi.org/10.3390/cells8090988

Zhu M, Liu J, Xiao J, Yang L, Cai M, Shen H, Chen X, Ma Y, Hu S, Wang Z, Hong A, Li Y, Sun Y, Wang X. 2017. Lnc-mg is a long non-coding RNA that promotes myogenesis. *Nature Communications* **8**:14718. DOI: https://doi.org/10.1038/ncomms14718, PMID: 28281528

Zuckerman B, Ulitsky I. 2019. Predictive models of subcellular localization of long RNAs. *RNA* **25**:557–572. DOI: https://doi.org/10.1261/rna.068288.118, PMID: 30745363

Desideri F, Cipriano A, Petrezselyova S, Buonaiuto G, Santini T, Kasparek P, Prochazka J, Janson G, Paiardini A, Calicchio A, Colantoni A, Sedlacek R, Bozzoni I, Ballarino M. 2020. Intronic determinants coordinate charme lncRNA nuclear activity through the interaction with MATR3 and PTBP1. *Cell Reports* **33**:108548. DOI: https://doi.org/10.1016/j.celrep.2020.108548, PMID: 33357424